# APPLICATIONS OF FT-INFRARED SPECTROSCOPY AND FT-RAMAN SPECTROSCOPY AS ANALYTICAL TOOLS

STEWART MEEHAN

Master of Philosophy

APRIL, 1999

UNIVERSITY OF SOUTHAMPTON

ABSTRACT

FACULTY OF SCIENCE
CHEMISTRY

Master of Philosophy

APPLICATIONS OF FT-INFRARED SPECTROSCOPY AND FT-RAMAN SPECTROSCOPY AS ANALYTICAL TOOLS

by Stewart Meehan

Infrared spectroscopy and Raman spectroscopy are invaluable analytical techniques used for a wide range of applications. The simple and versatile nature of the techniques provides analytical scientists with methods to determine parameters such as the identification of molecules and studies of crystallinity.

The work presented in this thesis is concerned with the use of firstly, infrared spectroscopy to study the polysulfide sealants currently used in the aerospace industry, and secondly, the use of Raman spectroscopy to study the polymers polypropylene and poly(ethylene terephthalate) at high temperatures.

Chapters 3 and 4 deal with the study of the degradation of polysulfide sealants. The fact that vibrational spectroscopy is a standard method of analysing degradation products and processes is emphasised. Polysulfide sealants as used in the aerospace industry, degrade over their lifetime resulting in costly repairs. In chapter 3 the chemistry of polysulfides and the factors, such as pretreatment of the adherend, which affect adhesion are introduced. Evidence is provided of cutting fluids remaining on the adherend after methods used to remove such fluids have been applied. An understanding of the degradation process in polysulfide sealants will lead to a better understanding of how to improve the sealants in the future. Chapter 4 puts forward a method for accelerating degradation testing of sealants.

Chapter 5 reports the first FT-Raman spectra of the polymers polypropylene and poly(ethylene terephthalate) above 200 °C. Observation of regularity bands and short range order at temperatures above the melting points lends credence to the arguments for a mesomorphic phase in the polymers.

# Acknowledgements

I would like to take this opportunity to thank the following who have made possible this, at times elusive, achievement :

my supervisor, Prof. Patrick Hendra for his invaluable supervision, support, encouragement and proof reading,

the international group of struggling scientists that I was lucky enough to have been a part of during my time at Southampton,

my friends in Southampton who introduced me to the delights of different cultures,

those I have since forgotten but who, indubitably, were of great aid and assistance in the Department of Chemistry,

lastly, my parents, whose love and understanding I will never be fully thankful for, nor understand.

# Table of Contents

# Chapter 1

# Introduction

# Chapter 1

# Introduction

## 1.1 General Introduction

Infrared and Raman spectroscopic techniques have been invaluable as analytical tools for many years. It is through the arrival of firstly Fourier-transform infrared spectroscopy (FT-IR) and in recent years Fourier-transform Raman spectroscopy (FT-Raman) that these methods have become quick, accurate and simplified. The study of rotation, vibration and rotation-vibration energy changes is possible using the techniques. The work presented in this thesis is mainly concerned with some of the uses of infrared and Raman vibrational spectroscopy as analytical tools.

The use of infrared spectroscopy and Raman spectroscopy as analytical tools is an ever expanding field with new applications being discovered regularly. Indeed so large is the field that many areas of infrared and Raman analysis such as, for example, polarisation studies are outside the scope of this thesis and are therefore ignored.

## 1.2 Fourier-transform spectroscopy

In conventional spectroscopy sweeping through all the frequencies being examined produces a spectrum. This is both time consuming and time wasting. There are a number of advantages of Fourier-transform instruments over the conventional ones. Fourier-transform spectroscopy provides a recording of the frequencies of the entire spectrum almost instantaneously (refer to Chapter 2). Taking the emitted radiation from an excited molecule as a sum of cosine waves an interferogram is produced. The interferogram arrives at the detector where the Fourier-transform processor converts the interferogram back into its frequency components, resulting in a frequency domain spectrum being produced. Noise occurring in the spectrum is reduced by scanning a number of times. The signal-to-noise ratio varies as $n^{\frac{1}{2}}$ where n = number

of scans. Therefore, as the number of scans increases the signal-to-noise ratio also increases, reducing the noise.

Averaging spectra will result in an improvement in the signal-to-noise ratio. For this to occur the spectra must be exactly superimposed upon each other. (In conventional instruments, the scanning monochromators wore and thus displacement errors were possible over time. This was eradicated in the 1970's.) In the Fourier-transform instruments a helium neon laser generates a reference frequency which does not vary. Thus, the spectra can be superimposed with great accuracy and averaged. This is known as the Connes advantage.

In conventional instruments the light is brought to a focus on a slit and thus the detector sees an image of this slit. The narrower the slit the better the resolving power of the instrument as the detector only receives a small range of frequencies at any one time. However the total amount of energy passing through the instrument is small and light is lost through reflection off mirrors and the diffraction grating. The étendue is used to compare optical efficiencies of instruments. The étendue is given by the product of the half angle of the cone of light collected and the area of the entrance aperture. The half angle of the cone of light collected is found by $\{\tan^{-1}[1/(2 \times f \text{ number of the collection optics})]\}$, where the f number is defined as the focal length divided by the diameter of the optical component. In a Fourier-transform spectrometer the light enters the interferometer through a large circular hole (typically 8mm in diameter for $4cm^{-1}$ resolution), known as the Jacquinot stop, as opposed to the slit system found in conventional instruments for the same resolution. Thus the area of the entrance aperture and therefore the étendue is much greater for a Fourier-transform instrument. This is known as the Jacquinot advantage.

Finally, in a Fourier-transform instrument all the wavelengths reaching the detector are recorded simultaneously and therefore a spectrum can be produced rapidly and continuously. Each detected element of an interferometer contains information about all wavelengths so there is a slight multiplex advantage known as the Felgett advantage. Therefore, it is possible to scan a number of times rapidly as opposed to a

conventional instrument, producing an improvement in the signal-to-noise ratio as discussed above.

## 1.3 Infrared Spectroscopy

Infrared spectroscopy is based on the absorption or transmission of energy by a sample. A continuum of radiation (in the range 400 to 4000 $cm^{-1}$ for mid-IR) from which the sample absorbs characteristic frequencies is used. Alternatively the infrared radiation emitted by a molecule in an excited state may be studied. For an infrared transition to occur there must be a change in the electric dipole moment of the molecule during a vibration. The intensity depends on the size of the dipole change. An infrared spectrum usually consists of a plot of wavelength ($\lambda$), or these days almost universally wavenumber ($cm^{-1}$), versus absorption or transmission. Infrared spectra reveal details such as vibrational frequencies, which provide evidence of certain groups in molecules, and internuclear distances.

### 1.3.1 Sampling Techniques

As glass absorbs infrared radiation the optical windows in an infrared spectrometer are usually made of materials such as KBr, which do not absorb infrared radiation. Solids, liquids and gases can be examined by infrared vibrational spectroscopy. In the case of solids some pretreatment is usually necessary in order to produce an infrared spectrum. The solid may have to be ground and then suspended in a suitable liquid which does not absorb strongly in the areas of interest of the infrared spectrum. Nujol and hexachlorobutadiene are usually the liquids used. The suspension or mull is then smeared between two KBr disks where the mull spreads out to a very thin film (0.1-10 mm thick). Thus the infrared spectrum can be recorded. The liquid used should be of similar refractive index to minimise light scattering. Another method of pretreating solids would be the pressed disk technique. The solid is ground up with KBr and then the mixture is subjected to pressure under vacuum. The KBr melts under the pressure and a transparent disk is formed. This then is placed in the sample compartment of a spectrometer and a spectrum can be recorded.

Reflectance techniques such as attenuated total reflectance (ATR), diffuse reflectance and specular reflectance can also be used. By their nature reflectance techniques are useful for examining the surfaces of solids. If the solid is flexible, (e.g. rubber), ATR can be used where the solid is pressed onto a crystal surface and the surface is then examined to a depth of $10^{-4}$-$10^{-3}$ cm using infrared radiation. Diamond crystal ATR allows uneven surfaced samples to be pressed under great force against the crystal surface in order to achieve good optical contact. For a detailed description of the ATR technique refer to chapter 2. Powders can be examined using diffuse reflectance infrared spectroscopy and solid reflective materials can be examined using specular reflectance techniques (also refer to chapter 2).

Liquids can be examined easily by smearing between two KBr disks. For quantitative work the liquids are placed into sealed cells of fixed path length. The molar absorption coefficient of a liquid can be calculated using the Beer-Lambert law:

$$I/I_0 = 10^{-\varepsilon cl} \ (= T, \text{ the transmittance})$$

where $\varepsilon$ is the molar absorption coefficient, c is the concentration of the liquid and l is the path length. I and $I_0$ are the detected intensity and the initial intensity respectively.

ATR can also be used to record the spectra of liquids where the liquid is simply dropped onto the crystal surface.

Gases are sampled using gas cells where the path length can vary considerably in length. Varying the pressure has the same effect as altering the length.

### 1.3.2 Infrared spectroscopy as an analytical tool

There is a plethora of reviews and papers in the literature highlighting the uses of infrared spectroscopy as an analytical tool. In the following pages some of these uses for a variety of situations are presented. In no way is this supposed to be a comprehensive catalogue of all uses of infrared spectroscopy. Indeed, whole books

have been written on the applications. Rather the aim is to expose a few of the different opportunities that infrared spectroscopy offers in the study of molecules. Degradation studies are somewhat focussed upon because the infrared work presented in this thesis is mainly concerned with this aspect.

Infrared has been used in the medical research world to study how the biological environment may affect implants. Changes in polymeric materials during implantation can affect the performance of the polymer. A study by Jacob *et al* used ATR-IR to follow the changes in performance of polymeric materials placed in rabbit eyes [1]. The ATR-IR spectra revealed protein deposition on all the examined polymers with the appearance of amide absorptions characteristic of proteins. ATR-IR clearly illustrated the absorption of proteins but as a protein can unfold differently on various surfaces, resulting in different IR spectra, it was not possible to identify the proteins. FT-IR also revealed significant changes in the polymer structure for some of the samples. Peaks were lost and new peaks appeared. The appearance of new peaks in the spectra was attributed to degradative changes in the polymer backbone chains.

These changes in polymer structure support the idea that polymer implant materials should be closely followed over several years *in vivo* in order to determine their suitability prior to use in humans. FT-IR provides a suitable method of following changes in the biological environment.

In a paper by Palmisano *et al* FT-IR was used to study the photodegradation of phenol on $TiO_2$ powders [2]. FT-IR was used as an *in-situ* analytical tool where an infrared cell allowed all thermal treatments of the $TiO_2$ and adsorption-desorption procedures to be carried out. Phenol was doped onto the $TiO_2$ powder. Under progressive irradiation by UV-visible light the bands in the IR spectrum of the adsorbed phenol decreased in intensity and new features appeared. This led to the conclusion that photodegradation of the phenol occurs at the surface. Using FT-IR Palmisano studied the effect of where increasing the presence of $H_2O$ and OH up to a limit of a monolayer appeared to increase the efficiency of the degradation of the phenol. Thus it was possible by using FT-IR to study the degradation and contributing factors for the phenol.

It has been published that the crystalline form of a protein drug is much more stable than the amorphous equivalent [3,4]. However, the use of FT-IR, as demonstrated by Pikal *et al,* proves that amorphous insulin is considerably more stable than crystalline insulin [5]. Pikal proposed that deamination of the crystalline insulin occurs when water is present, the rate increasing as the moisture rate increases. However, for amorphous insulin deamination is independent of moisture up to a water content of 15%.

Polytetrafluoroethylene powder partially degrades when irradiated with electrons. Irradiation produces COF groups with a band at 1884 $cm^{-1}$ due to the C=O stretching vibration [6]. The COF groups hydrolyse to carboxylic acid groups in the presence of water vapour [7]. A paper by Fischer *et al* describes the investigation of the influence of radiation dose and the hydrolysis conditions on the chemical structure [8]. Fischer used diffuse reflectance IR spectroscopy and transmission IR spectroscopy. It was clearly demonstrated that the concentration of the C=O groups rose due to increased radiation doses. In the diffuse reflectance spectra the bands of free (1810 $cm^{-1}$) and associated (1776$cm^{-1}$) acid groups were more intense than those seen for the transmission spectra. This, the authors argue, is due to the presence of higher amounts of the acid groups being present on the surface, hydrolysis being preferred there.

Diffuse reflectance was also used to study the thermal degradation of poly(ether ether ketone)-carbon composites [9]. The degradation process was found to be dependent on the atmosphere[10]. In an inert atmosphere a new carbonyl group appears at 1711 $cm^{-1}$. In an oxidising atmosphere the same group is detected but at a faster rate and also a new species absorbs at 1739 $cm^{-1}$.

Hong studied the degradation of a commercial epoxy adhesive on a metal surface using reflection absorption infrared (RAIR) spectroscopy [11]. The adhesive was spin-coated onto copper, interstitial-free steel (IFS) and aluminium polished surfaces and left to cure. The samples were then thermally degraded by placing in an oven at 125°C for a period of time. RAIR spectroscopy was used to follow the degradation process. Hong reports that degradation occurred quickest on the Cu surfaces and least quickly on the Al surface. He proposes that this is due to the amino based curing agents being preferably adsorbed onto the Cu surface.

Infrared analysis may be carried out on thin films. A paper by Molt *et al* demonstrates how thin inorganic and organic films on metals may be studied [12]. A phosphate coating on steel was examined. Molt used variable angle specular reflection IR spectroscopy to show the dependence of phosphate absorbance upon the angle of incidence. A unique angle of incidence was found which produced an optimum of sensitivity for surface profiling. This angle of incidence however is dependent on the surface thickness. As the thickness of the thin film decreases the optimum angle of incidence increases. Therefore the optimum angle of incidence for specular reflection may be used to predict the thickness of the film. Molt also demonstrated the use of reflectance IR for the identification and thickness measurements for organic thin films.

Timmins *et al* used ATR-IR to detect the enzymatic degradation of thin polymer films [13]. The film was poly(3-hydroxybutyrate-co-3-hydroxyvaerate) (PHBV), a naturally occurring copolyester produced by bacteria. The same bacteria also produce the enzymes with degrade the polymer. According to Timmins, degradation results in an increase in cystallinity at the film surface. This increase in crystallinity was verified with ATR-IR taking the ratio of crystalline-sensitive absorbance at 1382 $cm^{-1}$ to the crystalline-insensitive absorbance at 1185 $cm^{-1}$.

The semiconductor field is an extremely sophisticated and detailed area of research. The manufacture of semiconductor devices will often involve layering of new surfaces and the integrity of the previous surface is critical. A paper by Henry *et al* explores the use of FT-IR to analysis the surface degradation of InP during fabrication processes[14]. Fabrication processes on InP normally require temperatures rising up to 400 °C. Henry exposed the InP to gas (argon 80% / hydrogen 20%) at temperatures of 100, 200, 300 and 400 °C and studied any degradation than occurred using FT-IR. The results show that strong absorption changes occur after exposure at all temperatures. Henry proposes that the changes are due to loss of phosphorous from the surface which will result in an inferior device. Therefore FT-IR highlights an area of concern and provides necessary information with regard to degradation.

Mielczarski *et al* have used ATR-IR to study and characterise coal[15]. Knowledge of the structure of coal is important as technological processing such as coking and

liquefaction depend on it. Using ATR spectra samples of coal as large as 50 $\mu$m can be studied which are practically impossible to study in transmission spectroscopy. Transmission spectra also have the problems of water absorption of the KBr to contend with. Mielczarski also reports that low temperature oxidation of the coals at 130 °C in air was proceeded with, and the spectra were recorded. Therefore ATR-IR is a viable method to study the structure of coal.

The combination of thermogravimetric analysis and FT-IR (TGA/FT-IR) has proved a successful and convenient method of analysis. In a paper by Schild *et al*, TGA/FT-IR was used to study the thermal degradation of a polycarbonate [16]. The polycarbonate {poly(DMHD-CHD)carbonate}was heated to 200 °C where it began to degrade. The TGA shows a single sharp step indicating that degradation occurs in a single step. However the observed FT-IR spectrum displays changes with increasing temperature showing that the products do not evolve together. Schild identifies the products by a spectral library search. Therefore the use of TGA/FT-IR in determining the structure of degradation products is obvious.

- IR Vibrational Microscopy

Vibrational microscopy allows the examination of microscopic samples and thin films along with the advantage on being able to focus on regions of interest in a sample. Absorption-reflection experiments can be carried out on microscopic thin films on metal surfaces. However, a microscope is limited in the absorption-reflection mode as it cannot provide the variable angles that a macroscopic instrument permits. Surface contaminants can be studied without the interference of the background material. A paper by Thompson describes how a microscopic mark on a piece of paper was washed with methylene chloride onto an infrared window [17]. A transmission infrared spectrum of the residue indicated the presence of an aliphatic hydrocarbon characteristic of lubricants and thus the source of the blemish was traced to a leaking oil pipe involved in the manufacture of the paper.

The arrival of specialised ATR objectives for infrared microscopes has allowed the study of even more samples using vibrational microscopy. The sample is simply placed on the microscope stage and the objective is lowered until it touches the

sample. A paper by Hegemann *et al* demonstrates how an ATR objective lens on a vibrational microscope can be used to examine a thin film of lubricant oil metal surface after wear tests [18].

Surface profiling is possible using vibrational microscopy. This can be done by moving the microscope stage step-wise perpendicular to the objective lens and recording the IR spectrum after each step. Thus, factors such as crystallinity or content can be mapped. Both Raman and infrared microspectometry have been used to profile the surfaces of polymers and semiconductors [19-23].

Due to the ability to focus the infrared radiation (or laser in a Raman experiment) on a microscopic scale depth profiling is also possible. The sample is cut by microtoming [24] and the layers at the cut edge are examined. Using confocal techniques depth profiling has been reported for both infrared and Raman techniques [25-27].

Polymer blends are often processed at elevated temperatures. At these higher temperatures chemical reactions, crosslinking and experience of shear may occur. A paper by Manoj *et al* studies the affects of processing on PVC/NBR blends [28]. The blends were subjected to variables such as temperature, solvent swelling, presence of a PVC stabiliser and the speed of the mixing rotor. Infrared analysis was carried out on thin films of the blends. The infrared studies show the presence of thermally induced crosslinking at high temperatures and shear rates. The spectra show that the crosslinking reaction occurs in the presence of HCl which is a result of the degradation of PVC, through hydrolysis of the nitrile groups to form amide and ester crosslinks.

These examples demonstrate the versatility, and establish the choice of, Fourier-transform infrared spectroscopy as a routine analytical tool.

## 1.4 Raman Spectroscopy

Raman spectroscopy is concerned with light being scattered by a molecule. The scattered light at the incident frequency (almost all of the scattered light) is known as the Rayleigh scattering. However if an inelastic collision occurs, light striking the molecule may cause a rotational, vibrational or rotation-vibration change in the molecule. The scattered light now has a different frequency from the incident light the difference due to the energy change the molecule undergoes. If the molecule gains energy the scattered light will have lost energy and thus be at a lower frequency. If the molecule loses energy the opposite applies – thus the scattered light will be of a higher frequency compared with the frequency of the incident light.

The incident light is monochromatic and normally lies in the near infrared region of the spectrum for FT-Raman. The scattered light of lower frequency is usually the more intense as for the scattered light to be at a higher frequency than the incident radiation, the molecule must be in an excited state to begin. The lower frequency scattered light is known as Stokes radiation, that of the higher frequency is known as anti-Stokes radiation.

Raman spectroscopy depends on the "polarisability" of a molecule. This is discussed in more detail in chapter 2. Raman spectroscopy has a large advantage over infrared absorption in that little or no pretreatment of the samples is required. Samples are simply placed in a suitable holder so that they can be exposed to the incident radiation.

### 1.4.1 Sampling Techniques

Solids, for example plastics, are simply placed in the sampling area where the incident laser light strikes and the scattered light is collected.

Powdered samples are compacted into cells and placed in the path of the incident radiation. The cell consists of a hole in a darkened metal into which the powder is pressed.



Liquids are placed in silvered spherical glass cells or glass cuvettes. Usually glass does not produce a Raman spectrum but energy may be lost by reflection of radiation from the glass surface. Water, which absorbs strongly in the infrared, is a weak Raman scatterer and therefore it is possible to study solutions using visible incident light as the solvent does not swamp the signal. Problems may occur due to self-absorption. The scattered Raman light passing through the liquid sample may be reabsorbed producing a convolution of a Raman spectrum and a near-IR spectrum especially in the case of $H_2O$ which absorbs strongly in near-IR. $D_2O$ may be used as a substitute for $H_2O$ to avoid this occurring.

High temperature, low temperature, high pressure and low pressure experiments are easily carried out in suitable cells.

### 1.4.2 Raman spectroscopy as an analytical tool

As for infrared spectroscopy, Raman spectroscopy has many applications as an analytical tool. It is not the purpose of this thesis to provide a reference work for the world of Raman spectroscopy but rather to highlight some of the analytical aspects of Raman spectroscopy and to expose a few of the applications that have been published in the literature.

It should be remembered that the use of lasers as incident radiation in NIR FT-Raman spectroscopy results in a heating effect on the sample at the point of incidence. Obviously, this heating effect may result in unexpected phase transitions, e.g. melting, and/or decomposition may occur while a spectrum is being recorded. An examination of this heating effect and the amount of heating which can occur has been published by Pope *et al* [29]. In this study sodium molybdate, $Na_2MoO_4$, was examined using Raman spectroscopy. The $Na_2MoO_4$ was heated to 70 °C in a Ventacon hot cell and spectra were recorded for different laser powers. Other experiments carried out included keeping the laser power constant at 125 mW, the temperature of the sample at 70 °C and varying the number of scans, and also using a laser power of 250 mW, recording 5 scans at 20, 40, 60, 70 and 80 °C. $Na_2MoO_4$ undergoes a crystal transition at about 112 °C according to differential scanning calorimetry [30]. This transition in the sample is monitored using the peak at 896 $cm^{-1}$ in the spectrum. The temperature

was recorded for the bulk sample and did not show the temperature at the point of incidence of the laser. The results showed the following: sample heating increased as the laser power increased. The authors report that there is a substantial sample heating effect of at least 40 °C with the laser power set at 125 mW. At 80 °C the entire sample underwent a crystal transition in the 24 seconds required to record one scan.

Attempts to avoid the heating effect of the laser on the sample include using specially designed cells which will keep the sample cool; using a good thermal conductor such as KBr and a nujol mull to dissipate the heat from the sample, and rotating the sample so different sample areas are being exposed to the beam.

FT-Raman spectroscopy has been used to analyse pharmaceuticals and biomaterials and is especially effective for those which contain groups which are strong Raman scatterers such as phenyl groups and other aromatic constituents. A paper by Tudor *et al* describes the use of FT-Raman spectroscopy to differentiate between closely related compounds [31]. The fingerprint regions of the spectra revealed clear differences between three similarly structured drugs, arterenol, phenylephrine and ephedrine. Using a spectral library of known drugs it is possible to identify an unknown by simple comparison . The three drugs given in the example are chemically very closely related and yet are easily and quickly differentiated using Raman spectroscopy.

The paper also discusses the use of FT-Raman spectroscopy in establishing the kinetics of degradation for polymers. Spectra recording the degradation of poly(sebacic anhydride) in water were recorded over 150 days and clearly show decreases in intensity for the anhydride peaks whilst a peak at 1640 $cm^{-1}$, indicating an acid carbonyl group, emerges gradually. This follows the expected degradation path. As it is possible to identify the changes in the spectra as they occur the kinetics of the degradation process may be calculated.

A paper by Wang *et al* illustrates the use of Raman spectroscopy to study aspirin tablets [32]. The aspirin tablets were exposed to a moist atmosphere where the degradation of the aspirin results in the formation of salicylic acid. Comparison of the Raman spectra for the aspirin initially, aspirin after timed exposure to the moist

atmosphere and the spectrum of salicylic acid revealed the changes that occur in the aspirin spectra with time. HPLC measurements carried out on the same samples closely correlated the results attained. The only difference lay in the zero exposure time spectra that corresponded to the lowest salicylic acid content. The authors attributed the difference to the hydrolysis of the aspirin during the HPLC measurement.

The fact that hydrolysis occurs during the HPLC measurement shows an advantage of using the direct method of Raman spectroscopy to study the aspirin.

In another application of FT-Raman spectroscopy, Tait *et al* report the examination of two amine-based epoxy resin crosslinking agents [33]. The crosslinking agents are Mannich-based curing agent (MBCA) and epoxy amine adduct (EAA). Both of the crosslinking agents are highly coloured, samples which would have proved difficult to examine using conventional Raman spectroscopy. The authors recorded the spectra at 4 $cm^{-1}$ resolution and were able to propose assignments comprehensively for the peaks. They clearly identified spectral features which were unique to each of the crosslinking agents such as the antisymmetric oxirane stretching mode at 3055 $cm^{-1}$ and the stretching mode of $C(Me)_2$ species at 1380 $cm^{-1}$ in the EAA spectrum.

Raman spectroscopy has been used extensively in such fields as synthetic polymers where apart from qualitative studies, others such as crystallinity are also possible. In a paper by Agbenyega *et al* [34], emphasis is placed on the fact that the bands in Raman spectra are narrower than the equivalent bands occurring in infrared spectra. Thus, the authors argue that, meaningful Raman studies on crystallinity need to be made at high resolution, where highly crystalline species with half widths of 2-3 $cm^{-1}$ can be examined.

To conclude the illustration of examples, there are two very interesting and imaginative areas of research where Raman spectroscopy has been used as an analytical tool.

Firstly, Best *et al* demonstrate the use of Raman microspectroscopy to identify the pigments used in a 16$^{th}$ century German choir book [35]. Raman spectra were obtained on particles ranging from 3 to 30 μm and located in different regions that varied in colour. Malachite [$CuCO_3Cu(OH)_2$], vermilion (HgS), azurite [$2CuCO_3Cu(OH)_2$] and various lead pigments were identified from their Raman spectra. Furthermore, individual grains that under visual assessment appeared grey were shown by their Raman spectra to be a combination of lead white, carbon, vermilion, red lead and yellow pigments.

Secondly, Barry *et al* have used Raman spectroscopy to study the Ice-Man and contemporary skin [36]. The Ice-Man is a body of a young male who had remained in a glacial field in Oetzal between Austria and Italy for ~5200 years before being discovered. Remarkably, the body was intact upon discovery. The spectra of the skin from the Ice-Man and contemporary skin proved to be very similar in molecular structure. However some significant differences were noticed for example the N-H (amide-III) and C=O (amide I) deformation bands were dramatically decreased in intensity in the Ice-Man spectrum. The authors suggest this is a result of the protein 'bricks' in the skin having been degraded. This paper illustrates the ability of FT-Raman spectroscopy to non-destructively characterise important archaeological samples and also to demonstrate that degradation processes may be studied.

The above examples prove that FT-Raman spectroscopy is an extremely versatile and convenient method of analysis with far ranging applications.

## 1.5 Aims

The work presented in this thesis is concerned with the use of firstly, infrared spectroscopy to study the polysulfide sealants currently used in the aerospace industry, and secondly, the use of Raman spectroscopy to study the polymers polypropylene and poly(ethylene terephthalate) at high temperatures.

Chapters 3 and 4 deal with the study of the degradation of polysulfide sealants. The fact that vibrational spectroscopy is a standard method of analysing degradation products and processes is emphasised. An understanding of the degradation process in polysulfide sealants will lead to a better understanding of how to improve the sealants in the future. Chapter 4 puts forward a method for accelerating degradation testing of sealants.

Chapter 5 reports the first FT-Raman spectra of the polymers polypropylene and poly(ethylene terephthalate) above 200 °C. Observation of regularity bands and short-range order at temperatures above the melting points lends credence to the arguments for a mesomorphic phase in the polymers. This work was undertaken in collaboration with Dr. Andy Brookes at Southampton University.

## 1.6 Conclusion

The examples given in this chapter illustrate the versatility of Fourier-transform infrared spectroscopy and Fourier-transform Raman spectroscopy as analytical tools. Both methods are quick, accurate and relatively simple to use and can be used on a large variety of samples. The basis for the justification that these techniques should be used for the work described in this thesis is established.

## References:


1. J.T. Jacob, J.J. Lin, S.P. Mikal, *J.Biomedical Mat. Res.*, **37**, 4, (1997).
2. L. Palmisano, M. Schiavello, A. Sclafani, G. Matra, E. Borello, S. Coluccia, *Applied Catalysis B: Environmental*, 3, (1994).
3. M.J. Pikal, A.L. Lukes, J.E. Lang, K. Gaines, *J.Pharm.Sci.*, **67**, 767, (1978).
4. T. Oguchi, E. Yonemochi, K. Yamamoto, Y. Nakai, *Chem.Pharm.Bull*, **37**, (1989).
5. M.J. Pikal, D.R. Ringsbee, *Phar.Res.*, **14**, 10, (1997).
6. J.H. Golden, *Journal of Polymer science*, **39**, 534, (1960).
7. W.K. Fisher, J.C. Corelli, *Journal of Polymer Science, Polymer Chemistry Edition*, **19**, 2465, (1981).
8. D. Fischer, U. Lappan, I. Hopfe, K.-J. Eichhorn, K. Lunkwitz, *Polymer*, **39**, 3, (1998).
9. K.C. Cole, I.G. Casella, *Polymer*, **34**, 4, (1993).
10. K.C. Cole, I.G. Casella, *Thermochim. Acta*, referred to in reference [8].
11. S.G.Hong, *Angewandte Makromolekulare Chemie*, **215**, 73, (1994).
12. K. Molt, M. Egelkraut, K.-H. Gottwald, *Mikrochim Acta [Wien]*, II, (1988).
13. M.R. Timmins, D.F.Gilmore, N. Lotti, M. Scandola, R.C. Fuller, R.W. Lenz, *Journal of Environmental Polymer Degradation*, **5**, 1, (1997).
14. J. Henry, J. Livingstone, *Infrared Phy. Technol.*, **36**, 3, (1995).
15. J.A. Mielczarski, A. Denca, J.W. Strojek, *Applied Spectroscopy*, **40**, 7, (1986).
16. H.G. Schild, M.G. Horner, *Pure Appl.Chem.*, **A31**, 12 (1994).
17. M.M. Thompson, *Vibrational Spectroscopy*, **2**, 15, (1991).
18. B.E. Hegemann, S. Jahanmir, S.M. Hsu, *Microbeam Analysis-1988*, 193, (1988).
19. A. Kaito, M. Kyotani, K. Nakayama, *Polymer*, **33**, 2672, (1992).
20. T. Nishioka, N. Teramae, *Analytical Sciences*, **7**, 1633, (1991).
21. J. Jimenez, E. Martin, A.C. Prieto, A.Torres, *Semiconductor Science and Technology*, **7**, A288, (1992).
22. G. Abstreiter, *Applied Surface Science*, **50**, 73, (1991).
23. H. Tang, I.P. Herman, *Journal of Applied Physics*, **71**, 3492, (1992).
24. T.J.Allen, *Vibrational Spectroscopy*, **3**, 217, (1992).

25. R.J. Pell, M.L. McKelvey, M.A. Harthcock, *Applied Spectroscopy*, **47**, 634, (1993).
26. T. Jawhari, J.M. Pastor, *Journal of Molecular Structure*, **266**, 205, (1992).
27. T. Ozeki, D.E. Irish, *Journal of Physical Chemistry*, **96**, 1306, (1992).
28. N.R. Manoj, P.P. De, *Polymer*, **39**, 3, (1998).
29. S.J.A. Pope, Y.D. West, *Spectrochimica Acta : Part A*, 51, (1995).
30. M. Hanney, personal communication to Y.D. West, (1995).
31. A.M. Tudor, C.D. Melia, J.S. Binns, P.J. Hendra, S. Church, M.C. Davies, *Journal of Pharmaceutical and Biomedical Analysis*, **8**, 8-12, (1990).
32. C. Wang, T.J. Vickers, C.K. Mann, *Journal of Pharmaceutical and Biomedical Analysis*, 16, (1997).
33. J.K.F. Tait, H.G.M. Edwards, D.W. Farwell, J. Yarwood, *Spectrochimica Acta : Part A*, 51, (1995).
34. J.K. Agbenyega, G. Ellis, P.J. Hendra, W.F. Maddams, C. Passingham, H.A. Willis, J. Chalmers, *Spectrochimica Acta*, **46A**, 2, (1990).
35. S.P. Best, R.J.H. Clark, R. Withnall, *Endeavor*, **16**, 66, (1992).
36. A.C. Williams, B.W. Barry, H.G.M. Edwards, D.W. Farwell, F. Rull, *J.Chem.Soc. Faraday Trans.*, **91**, 21, (1995).

# Chapter 2

# Experimental Techniques

# Chapter 2

# Experimental Techniques

## 2.1 Introduction

The basis of both infrared and Raman spectroscopy is the vibrational motion of molecules. Each molecule possesses a vibrational fingerprint that enables the spectroscopist to identify the molecule and investigate the structural and morphological properties of the molecule.

It is important to discuss molecular vibrations and how they give rise to infrared and Raman spectra. There now follows a brief account of the fundamentals of the vibrational behaviour of molecules and the instrumentation that is used to detect this behaviour.

### 2.1.1 The vibrational behaviour of molecules

Atoms in a molecule are in constant motion, vibrating around an equilibrium position, in such a way that the centre of mass remains fixed and no rotation occurs. The simplest case, that of a diatomic molecule, can be represented by a spring with a force constant, k, connecting two masses, $m_1$ and $m_2$, together. A force, F, applied to either of the masses will result in a displacement by an amount x, such that:

$$F = -kx \qquad (1)$$

Thus, the vibrating molecule may be approximately modelled as a simple harmonic oscillator. The frequency $\nu_{vib}$ at which harmonic oscillation takes place is given by:

$$\nu_{vib} = \frac{1}{2\pi}\left(\frac{k}{\mu}\right)^{\frac{1}{2}} \qquad (2)$$

where $\mu$ is the reduced mass given by:

$$\mu = \frac{m_1 m_2}{m_1 + m_2} \quad (3)$$

From quantum theory the energy associated with the simple harmonic oscillator is quantised into a series of energy levels. The energy levels have values of:

$$E_v = h\nu(V+{}^1/_2) \quad (4)$$

where V is the vibrational quantum number = 0,1,2,...

These energy levels are separated by:

$$\Delta E = h\nu \quad (5)$$

The energy of the lowest level is $h\nu/2$. Therefore, the molecule is always vibrating.

### 2.1.2 Anharmonicity

The simple harmonic model is, however, only an approximation. It does not allow for the molecule's dissociation. Real molecules are anharmonic vibrators. A more accurate representation of the potential energy versus displacement curve is described by the "Morse function":

$$E = D_{eq}[1-\exp\{a(r_{eq}-r)\}]^2 \quad (6)$$

where $D_{eq}$ = dissociation energy, $r_{eq}$ = equilibrium bond length, r = internuclear bond distance and a = constant characteristic of a particular electronic state of the molecule. A comparison between the potential energy curves expected for the simple harmonic oscillator and the Morse function is shown in **Figure 2.1**

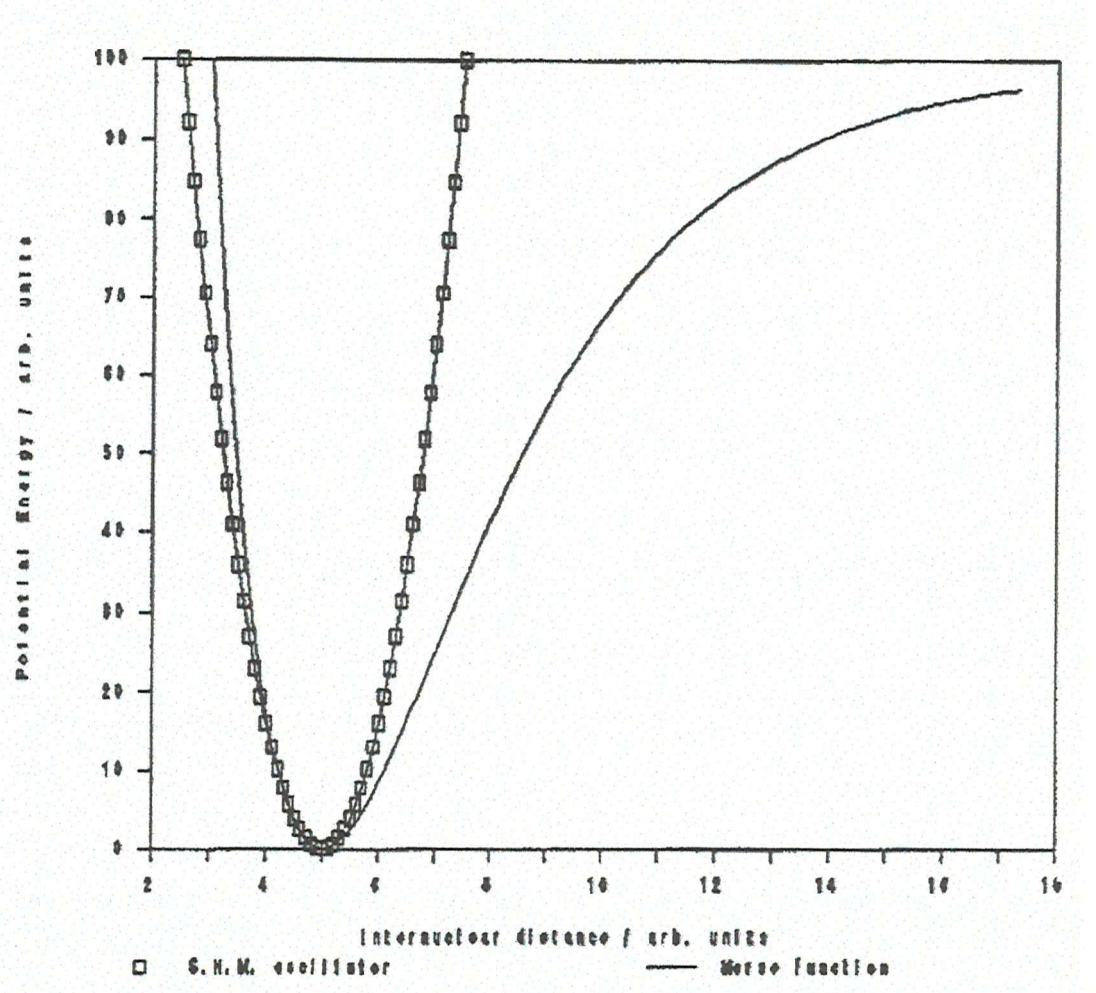


**Figure 2.1:** *Plot of internuclear distance versus potential energy for a simple harmonic oscillator and a molecule obeying the Morse function.*

The expression for the quantised vibrational energies now becomes:

$$E_v = h\nu[(V+{}^1/_2) - (V+{}^1/_2)^2 X_e] \qquad (7)$$

indicating that the levels are not equidistant but rather become closer as V increases.

For a molecule of 'N' atoms there are 3N independent degrees of freedom corresponding to 3 translations, 3 rotations (or 2 if a linear molecule), and the remaining 3N-6 (3N-5 for a linear molecule) result in vibrational motion. These vibrations are referred to as the fundamental modes of vibration and may be described precisely for each individual molecule.

Taking $CO_2$ as an example there must be 3N-5 = 4 modes of vibration. These are represented by :

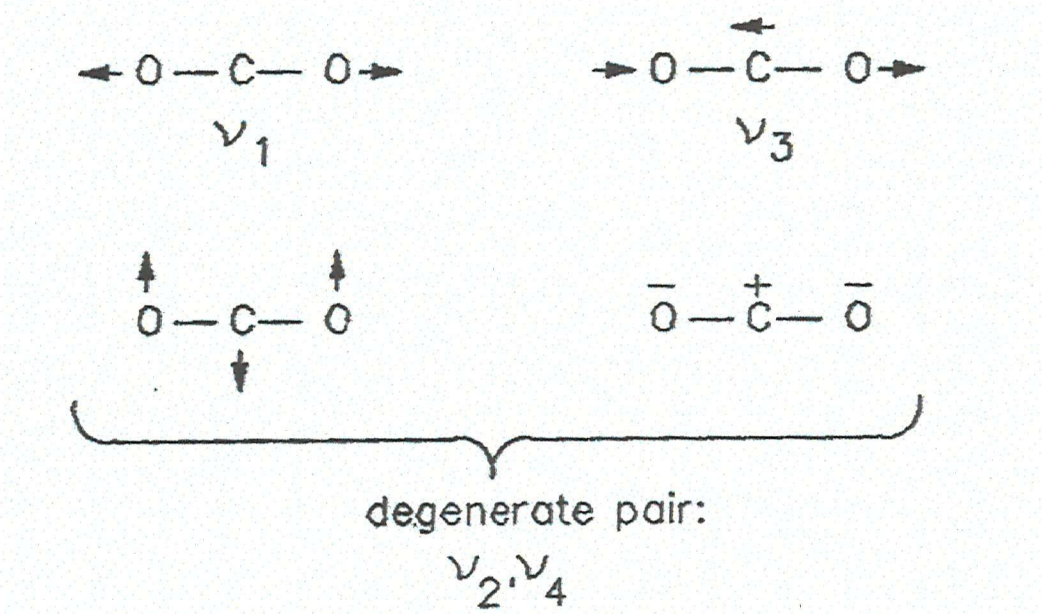


**Figure 2.2:** *$CO_2$ modes of vibration (all other motions are combinations of these or involve translation of the centre of mass or rotation about it).*

### 2.1.3 Infrared Activity

For a molecular vibration to be infrared active there must be a change in the molecule's dipole moment. This is expressed as:

$$\frac{\delta\mu}{\delta q} \neq 0 \qquad (8)$$

where $\mu$ = dipole moment and q = normalised co-ordinate.

If the vibration results in a change in dipole moment then electromagnetic radiation equal to $\Delta E$ can interact with the vibration and absorption or emission of radiation may take place. This can be clearly be seen as demonstrated for the vibrations of $CO_2$ in Figure 2.3.

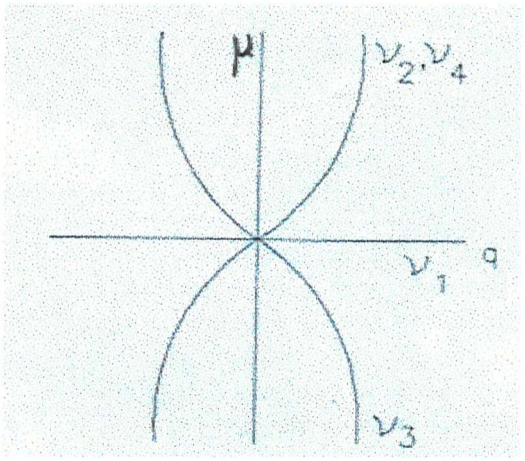


**Figure 2.3:** *Plot of dipole moment versus q of vibrational modes of $CO_2$.*

Molecular vibrations resulting in absorption or emission of radiation occur in the range from 100 $cm^{-1}$ to 4000 $cm^{-1}$ of the electromagnetic spectrum, the infrared region.

### 2.1.4 Raman Activity

When a molecule experiences an electric field, E(V/m), a dipole, P(V/m) can be induced whose magnitude will depend on the polarisability constant, $\alpha$, of that molecule such that:

$$P = \alpha E \tag{9}$$

If the electric field is oscillating as it does in electromagnetic radiation and has frequency, $\nu_o$(Hz), the field can be represented by:

$$E = E_o \cos(2\pi\nu_o t) \tag{10}$$

where $E_o$ = maximum value of field strength, and t = time. Thus

$$P = \alpha E_o \cos(2\pi\nu_o t) \tag{11}$$

The excited molecule will itself be vibrating at a fixed frequency, $\nu_{vib}$ (Hz), oscillating about the equilibrium bond length:

$$q = q_o \cos(2\pi\nu_{vib}t) \quad \textbf{(12)}$$

where q = progress through the vibration from the equilibrium position to a maximum of $q_o$. This displacement can cause a change in the polarisability of the molecule which will be effected according to:

$$\alpha = \alpha_0 + \left(\frac{\delta\alpha}{\delta q}\right)_0 q_0 \cos(2\pi\nu_{vib}t) \quad \textbf{(13)}$$

and substituting this expression for α into equation 11 gives:

$$P = \alpha_0 E_0 \cos(2\pi\nu_0 t) + \left(\frac{\delta\mu}{\delta q}\right)_0 q_0 \cos(2\pi\nu_{vib}t)\cos(2\pi\nu_0 t) \quad \textbf{(14)}$$

This can be simplified using:

$$\cos A.\cos B = \tfrac{1}{2}[\cos(A+B)+\cos(A-B)] \quad \textbf{(15)}$$

to give:

$$P = \alpha_0 E_0 \cos(2\pi\nu_0 t) + \frac{1}{2}\left(\frac{\delta\alpha}{\delta q}\right)_0 q_0 [\cos\{2\pi(\nu_0 + \nu_{vib})t\} + \cos\{2\pi(\nu_0 - \nu_{vib})t\}] \quad \textbf{(16)}$$

$\nu_0$, $\nu_0+\nu_{vib}$, and $\nu_0-\nu_{vib}$ vary. Therefore, so will the induced dipole. Light will be emitted or scattered at those frequencies. Rayleigh scatter ($\nu_0$) is elastic, i.e. it occurs at the same energy as the incident radiation. The $\nu_0+\nu_{vib}$ and $\nu_0-\nu_{vib}$ terms are known as anti-Stokes Raman scatter and Stokes Raman scatter respectively. The following diagram shows the transitions involved:

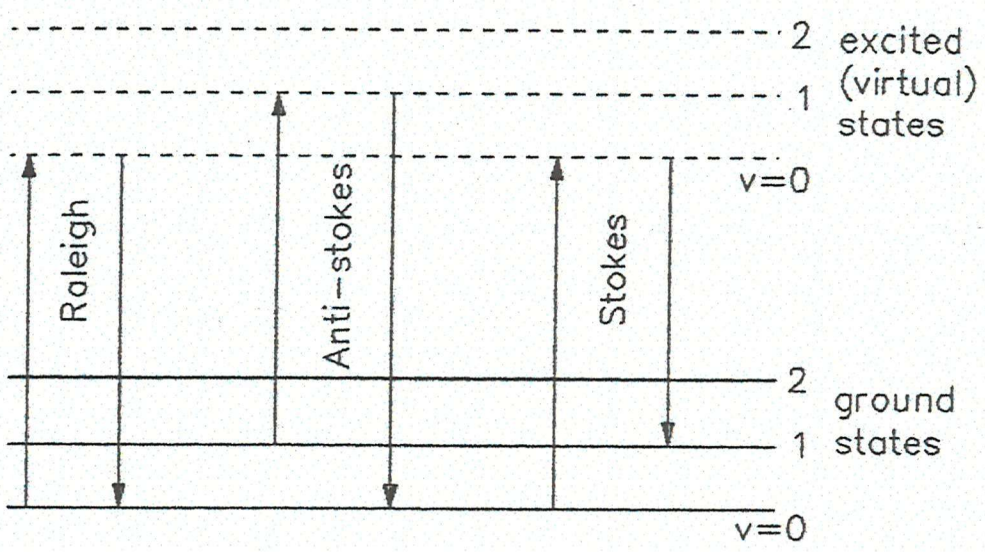


**Fig.2.4** *Diagram of Stokes, anti-Stokes and Rayleigh lines.*

The relative intensity of the Stokes and anti-Stokes scatter depends on the populations of the ground state and the first excited vibrational state. These are given by the Boltzmann distribution:

$$\frac{n'}{n} = \frac{g'}{g}\exp\left(\frac{-\Delta E}{kT}\right)$$

where n is the population, g is the degeneracy and ′ denotes the upper level.

Due to the fact that it is the Stokes scatter which is more intense and complete (the anti-Stokes only appears at low frequencies), it is the Stokes side which is scanned normally. The selection rule for a vibration to be Raman active is that a finite change in polarisability occurs. This is demonstrated in Figure 2.5, which again uses carbon dioxide as an example. Here, $\nu_1$ displays a large change in polarisability and hence is Raman active. The vibrations $\nu_2$, $\nu_3$, $\nu_4$ display only a minimal change and therefore are not Raman active.

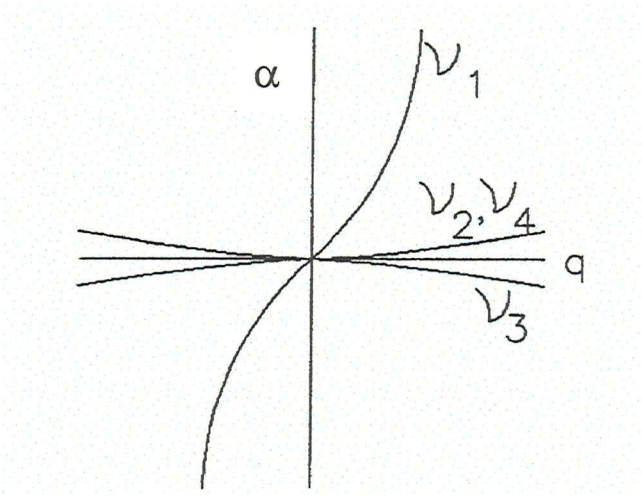


**Figure 2.5:** *Plot of polarisability versus q*

It should be noted that centrosymmetric molecules display the property *of mutual exclusion* whereby modes of vibration visible in the infrared spectrum are not present in the Raman spectrum and vice versa. The example of carbon dioxide used in the figures above demonstrates this clearly.

## 2.2 Techniques and Instrumentation

The main techniques used in this thesis were Fourier-transform infrared spectroscopy and Fourier-transform Raman spectroscopy. There follows a brief description of the instruments used and the principles behind them.

### 2.2.1 The Michelson interferometer

At the centre of Fourier-transform infrared and Raman spectrometers is an interferometer based on the Michelson interferometer.

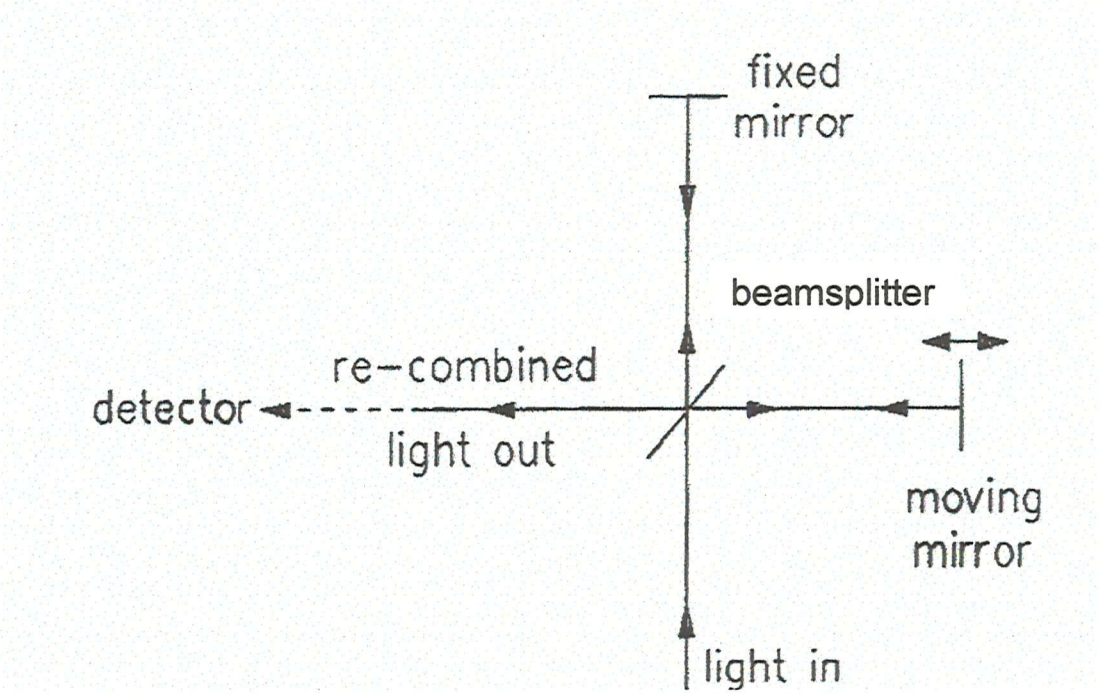


**Figure 2.6:** *Michelson interferometer*

For a monochromatic source, a ray of light strikes the beamsplitter which is usually made of KBr and semi-coated with reflective material. The coating is put on in such a way that half of the light is reflected and the other half is transmitted. Figure 2.6 shows the components involved. Thus, half of the light strikes the fixed mirror ($M_1$) and the other half strikes the moving mirror ($M_2$) resulting in an optical delay. As $M_2$

is moving the light reflected back to the beamsplitter may have a changed path length. Therefore, interference between the reflected rays can occur. Constructive interference will occur when the difference in path lengths of the recombining light rays is a wavelength or they differ by an integral number of wavelengths. Destructive interference will occur when the difference in path lengths is a half-integral number of wavelengths. Thus for an infrared source an interference pattern results and an interferogram is produced at the detector. A computer can carry out a Fourier-transform on the interferogram producing a spectrum showing the frequencies and intensities emitted by the source. A helium-neon laser passing through the interferometer provides a precise reference wavelength with which the interferogram can be Fourier-transformed.

### 2.2.2 Infrared Spectrometer

In the infrared spectrometer the sample is placed in the beam path as shown in Figure 2.7. The sample will absorb characteristic frequencies of light. Thus when the interferogram is converted into a spectrum these frequencies will be displayed as downward peaks. These peaks are characteristic of the group of atoms present and therefore the structure may be determined.

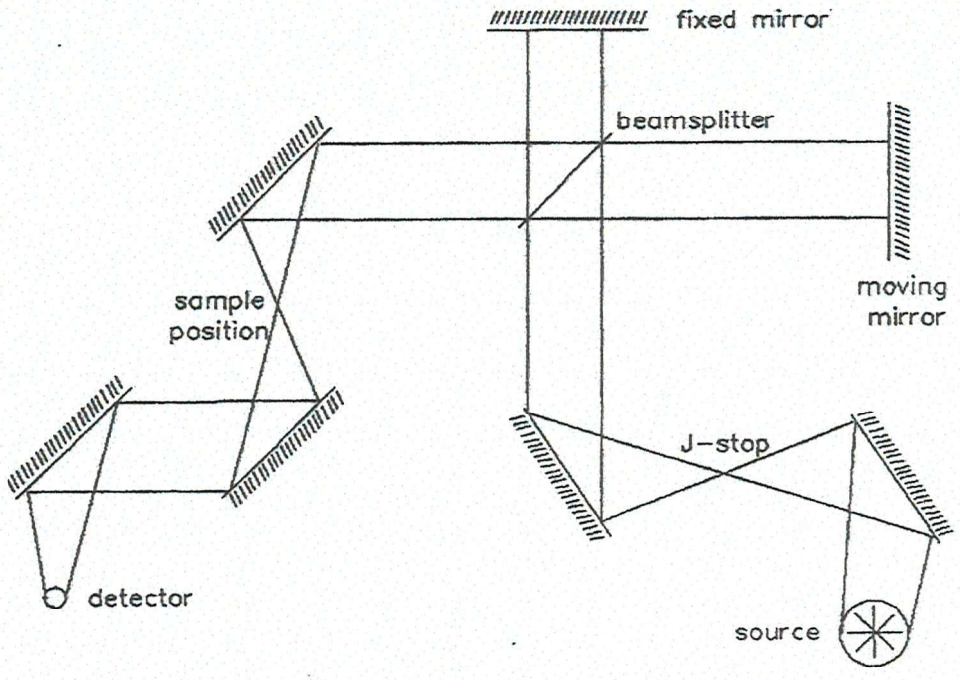


**Figure 2.7:** *Schematic representation of an infrared spectrometer.*

The infrared source is usually a filament heated using an electric current. Two examples would be the old Nernst filament which is a rod 2-5 cm in length and ~2 mm in diameter, consisting of 90 parts by weight zirconium oxide, 7 parts yttrium oxide, and 3 parts erbium oxide. It is necessary to preheat the Nernst filament using an external electric heater. Temperatures reach ~2000 K. The globar filament, which is essentially a rod of carborundum (silicon carbide), conducts electricity at room temperature and therefore no preheating is required. Temperatures reach >1500 K.

Detectors commonly used are the deuterated triglycine sulphate (DTGS) detector and the mercury cadmium telluride (MCT) detector which is cooled to –180 °C.

A variety of techniques exist for gathering the FTIR spectra. Methods used in this work included ***attenuated total reflectance*** and ***specular reflectance***.

### 2.2.3 Attenuated total reflectance (ATR)

If radiation travelling through a crystal of high refractive index ($n_1$) impinges on an interface where the second medium (sample) is of significantly lower refractive index ($n_2$), and the angle of incidence is greater than the critical angle, the radiation will be reflected at the interface. Even though there is total reflection, the radiation does travel outside the crystal penetrating the medium of smaller refractive index for a very short distance (of the order of microns). Therefore, it is possible to obtain a spectrum for this phase by recording the reflection coefficient, $R = I_R/I_O$, as a function of the wavelength of the incident beam. The depth of penetration into the medium of smaller refractive index depends on the optical properties of the system, $n_1$, $n_2$, $k_2$ (where $k_2=2\square n_2/^{8}$); on the value of the angle of incidence, $\Phi$ (Fig.2.8); and on the wavelength of the radiation.

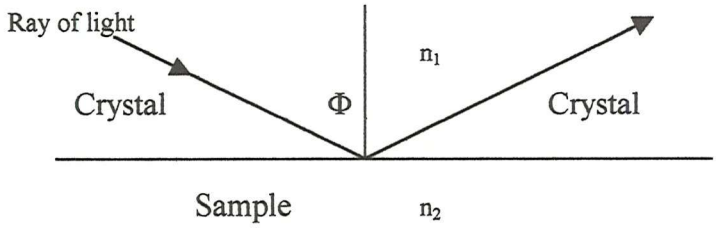


**Figure 2.8.**

$$dp = \frac{1}{k_2\sqrt{[(n_1 / n_2)\sin\Phi]^2 - 1}}$$

The intensity of the bands in the reflection spectrum depends on the same variables. The amplitude of the electromagnetic wave, E, penetrating the phase investigated, decreases exponentially with the increase of the distance from the interface:

$$E = E_o e^{-Z/dp}$$

where $E_o$ is the amplitude of the electromagnetic wave at the interface, Z is the distance from the interface in the less dense phase, and dp is the depth of penetration. Therefore, the reflected beam carries information concerning mainly the surface layers of the sample. In order to increase the intensity of the bands in the reflection spectrum of the sample, multiple reflections are used.

### 2.2.4 Specular reflectance

When the sample has a very smooth, plane surface, the specular reflectance spectrum is obtained by directing the infrared beam onto the sample surface and recording the reflected energy when the angle of reflection is the same as the angle of incidence. When the sample under study is a thin coating on a metal substrate, the specular reflectance spectrum recorded is predominantly an absorption one. The reflection spectra exhibit infrared bands whose shapes resemble first derivatives as the spectra are plots of the reflection coefficient versus frequency. By using the Kramers-Kronig dispersion formulae these spectra can be converted into transmission-like spectra. The Kramers-Kronig dispersion relation is given by :

$$\theta(E) = -\frac{2E}{\pi} P\int_o^\infty \frac{\ln\rho(E')}{(E')^2 - E^2} dE$$

where $\rho(E)$ is the reflected amplitude, $\theta(E)$ is the reflected phase, $R(E)= \rho(E)e^{i\theta(E)}$ is the complex reflectance and $\rho(E)^2$ is the measured reflectance. The reflectance amplitude is measured and using the Kramers Kronig analysis the phase is obtained by a Fourier-transform approach.

All of the infrared spectra recorded in this thesis were recorded on a 1700 series Perkin Elmer Fourier-transform infrared spectrometer, at 4 $cm^{-1}$ resolution with 25 scans (or sufficient for the signal to noise ratio to reach an acceptable level) being recorded for each spectrum. The source was a voltage stabilised, air cooled ceramic operating at 1400 K and the detector was a DTGS.

### 2.2.5 Raman Spectrometer

A laser in used in a Raman spectrometer to excite the molecules and produce the scattered radiation. Usually spectrometers use a $Nd^{3+}$YAG laser, which operates at 1064 nm. Figure 2.9 shows a schematic representation of a Raman spectrometer. The laser beam is reflected off the prism onto the sample and the resultant scattered radiation is gathered by the collection optics. This collected scattered radiation is then passed through an interferometer before reaching the detector. The Rayleigh light is removed by a series of filters. The beamsplitter differs from that of the infrared spectrometer in that it is usually made of quartz or $CaF_2$ to allow frequencies in the range 9400-5400 $cm^{-1}$ to be transmitted. Also, at these frequencies the detector used is usually an indium gallium arsenide photo-resistor.

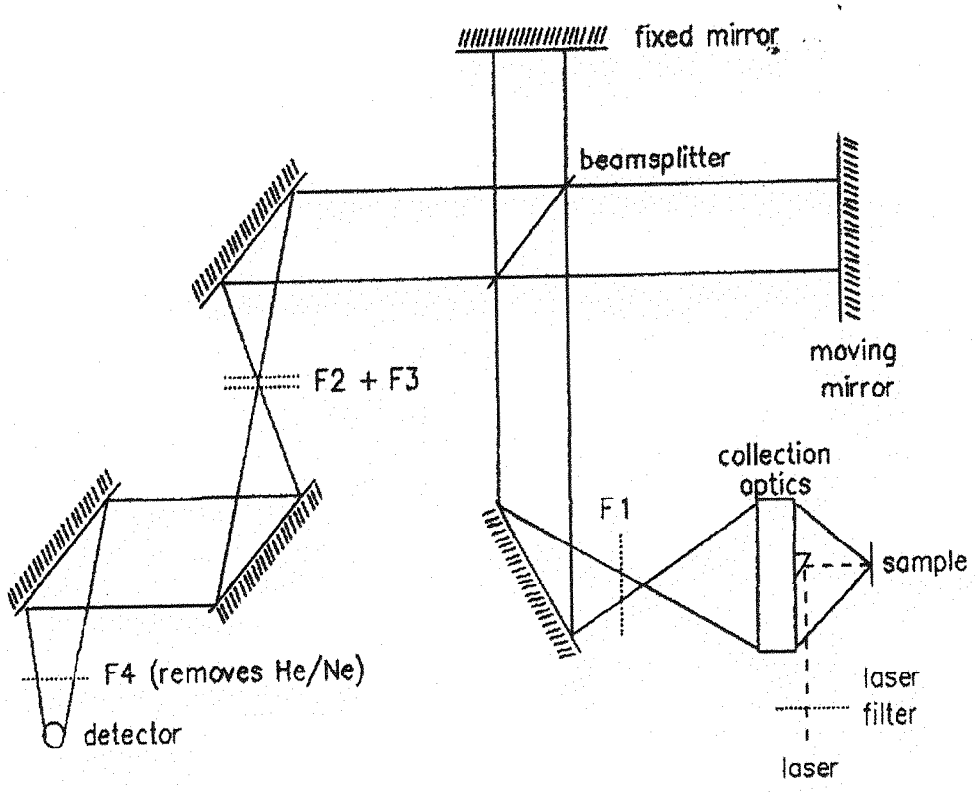


**Figure 2.9:** *Schematic representation of Raman spectrometer.*

All Raman spectra recorded in this thesis were carried out at 4 $cm^{-1}$ resolution using a neodymium-doped yttrium aluminium garnet crystal ($Nd^{3+}$YAG) excitation laser emitting continuous wave laser radiation at a wavelength of 1064 nm (9398 $cm^{-1}$). The detector was an Indium Gallium Arsenide (InGaAs) version. Usually, 25 scans were recorded or until the spectrum displayed an acceptable signal-to-noise ratio.

**References:**


1. P.J. Hendra, C. Jones, G. Warnes, *Fourier-transform Raman Spectroscopy (Instrumentation and Chemical Analysis)*, published by Ellis Harwood, 1991.
2. C.N. Banwell, E.M. McCash, *Fundamentals of Molecular Spectroscopy (4$^{th}$ Ed.)*, published by McGraw-Hill Book Company, 1994.
3. T. Smith-Palmer, B.M. Lynch, C. Roberts, Y. Lu, *Applied Spectroscopy*, **45**, 6, (1991).
4. M.L. Bortz, R.H. French, *Applied Spectroscopy*, **43**, 8, (1989).
5. T. Buffeteau, B. Desbat, D. Eyquem, *Vibrational Spectroscopy*, **11**, 1, (1996).
6. P.A. Wilks, *Applied Spectroscopy*, **22**, 6, (1968).

# Chapter 3

# Characterisation of the Sealant PR1422 B2

# Chapter 3

# Characterisation of the sealant PR1422 B2

## 3.1 Introduction

The work in this chapter and chapter 4 is concerned with a study of the sealants used in the fuel tanks of aircraft. The sealants currently in use deteriorate over the service life of the aircraft. This results in costly repairs and aeroplane downtime losses. It is the aircraft manufacturers who have to cover the expenses incurred. Obviously a solution to the sealant problem is required.

This chapter introduces the manufacture and composition of the sealants used in the aerospace industry. The variables that make up the seal are characterised namely; the primer painted substrates, the sealants and the fuel.

### 3.1.1 Sealants

Sealants should be impervious to the diffusion of liquids and gases. Sealants are commonly found in today's industries. In order to be effective, a sealant must have good chemical resistance, high adhesive and cohesive strength and also flexibility over a wide range of service conditions. One important use of sealants is in the sealing of aircraft fuel tanks. In the operation of aircraft sharp extremes of temperature varying between –50 °C to 120 °C within a few minutes are incurred, and the adhesive sealant must be able to cope. A sealant should seal in spite of changes in temperature, humidity and other environmental factors. A ninety-feet wing may flex sixteen feet vertically under operating conditions and the sealant must have the flexibility to facilitate this movement [1].

Today's aircraft require great amounts of fuel. Both space and weight are critical factors. In the early days of aviation, cavities were left within the wings or fuselage into which large sealed fuel bags or tanks were placed. Nowadays, it is the wings and fuselage themselves which form the fuel tanks, i.e. the tank is an integral part of the aircraft. Therefore, it is necessary to seal every rivet and joint to prevent leakage.

### 3.1.2 Polysulfide liquid polymers

For many years polysulfide liquid polymers have been the basic raw material used in the manufacture of sealants for aerospace applications. In 1928, Dr. J. Partick mixed ethylene dichloride and sodium polysulfide producing a material similar to natural rubber [2]. That the material was also oil and petrol resistant was of great interest. In 1943 after increased research work on polysulfide materials, the first liquid polysulfide was produced [2]. Using appropriate curing agents it could be cured from a liquid to a rubber at room temperature. This liquid polysulfide formed the basis of the polysulfide materials currently in use as sealants throughout industry today. (*The Vickers Supermarine 'Swift' was the first aircraft in the U.K. to be sealed with a polysulfide polymer).*

Today, polysulfide systems are used extensively in the aerospace industry due to their high resistance to aliphatic hydrocarbon solvents and their outstanding performance over a wide range of temperatures endured during flight. They have exceptionally good tensile and elongation properties and, with the aid of adhesion promoters and/or a primer, will show extremely good adhesion to a variety of surfaces. Although the resistance of polysulfides to aviation fuel is excellent, their resistance to water is modest. Unfortunately, large amounts of water are present in the integral fuel tanks.

### 3.1.3 Manufacture and Composition of Polysulfide Sealants

Dichlorodiethylformal, $Cl\text{-}C_2H_4\text{-}O\text{-}CH_2\text{-}O\text{-}C_2H_4\text{-}Cl$, is used as the main monomer in the manufacture of today's polysulfide sealants [3]. Sodium polysulfide, $Na_2S_x$, is added and reacts in aqueous suspension. This results in the production of a high molecular weight polysulfide.

$$nCl\text{-}R\text{-}Cl + nNa_2S_x \rightarrow (\text{-}R\text{-}S_x\text{-})_n + 2nNaCl$$

where R is $C_2H_4\text{-}O\text{-}CH_2\text{-}O\text{-}C_2H_4$

The above polysulfide is then partially depolymerised, or desulphurised, resulting in lower molecular weight liquid polymers. Sodium sulfite and sodium hydrogen sulfide are used to reduce some of the polysulfide groups to thiol and disulfide groups [4].

$$\sim RSSSR\sim + Na_2SO_3 \rightarrow \sim RSSR\sim + Na_2S_2O_3$$

$$\sim RSSR\sim + NaSH \rightarrow \sim RSH + NaSSR\sim$$

$$\sim RSSNa + Na_2SO_3 \rightarrow \sim RSNa + Na_2S_2O_3$$

As a consequence of the above process, polymers with RSNa terminal groups are produced. The average molecular weight of these polymers is controlled by the quantity of sodium salts added. The low molecular weight fraction is soluble in the aqueous phase but the higher molecular weight fraction forms a dispersion.

Acidification of the mixture results in coagulation of the dispersed polymer and the soluble polymer precipitates out. A mercaptan and disulfide interchange procedure produces a less varied molecular weight distribution. This process continues during washing, drying and storage of the liquid polymer. In order to produce a branched chain polymer a small amount of a trifunctional species, for example, 1,2,3-trichloropropane, $C_3H_5Cl_3$, is added to the polymer mixture [5]. Crosslinking results in a polymer which has the advantage of much greater strength and more rigidity. The pH of any additives to the sealant has to be carefully regulated, as a decrease in pH nay result in a retardation of the curing rate [3].

Polysulfide sealants used in the aerospace industry are two-part room temperature vulcanising systems, comprising of

**1 :** the base

**2 :** the curing agent.

**The Base :** The base usually contains the liquid polymer, fillers, plasticisers, solvent and adhesion promoters. The filler is added to enhance the properties of the sealant, reduce the cost and colour the sealant. The particle size of the filler is an important factor. A filler of small particle size (100-200 Å) increases the strength and thixotropy

of the sealant. The most commonly used are carbon black, titanium dioxide and silicas, all of which increase the tensile and tear strength of the sealant and, calcium carbonates and clays, which are used to increase the thixotropy. Thixotropic agents are used to avoid 'sagging' of the adhesive [1]. Carbon black is also used to adsorb ultra-violet radiation.

Plasticisers are used to enhance the plastic properties of the sealant, improve the resistance to oils and minimise cracking [6]. Common examples would be dibutyl-phthalate and certain phenylalkanes [7] of general structure:

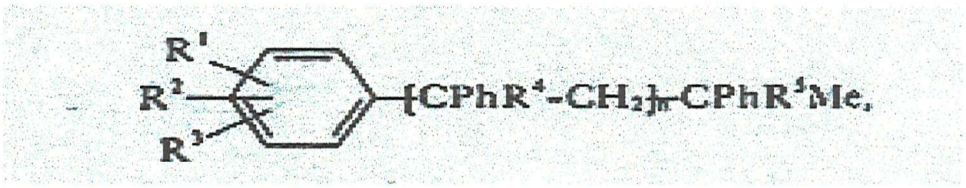

where $R^1$, $R^2$ = Me, $R^3$ = H, $R^4$, $R^5$ = H and n = 1.

Other plasticisers used are chlorinated paraffins and coal tar fractions of high aromatic proportion. Care must be taken with regard to the amount of plasticiser added as too much may result in lowering the tear resistance and adhesion properties.

Toluene is the usual solvent and is used to disperse the resin.

To improve the adhesion of the polysulfides adhesion promoters are added. The adhesion promoters most commonly used are phenolic resins with active methylol groups, (which strongly adhere to airframe metals, show good fuel resistance and are compatible to reinforcing fillers), bisphenol based epoxide resins, (used in $MnO_2$ cured systems), silane compounds and titanates [8]. These can slowly react with the -SH groups on the polymer chain. For example the epoxide may react as follows [9] :

$$\sim R'SH + RCH\text{-}CH_2 \rightarrow \sim R\text{-}CH\text{-}CH_2\text{-}S\text{-}R'$$
$$\qquad\quad O \qquad\qquad\quad OH$$

Phenolic resins may inhibit the cure of the sealant, especially the $MnO_2$ system, as they are slightly acidic in nature. The phenolic resin can react as follows [8-2852]:

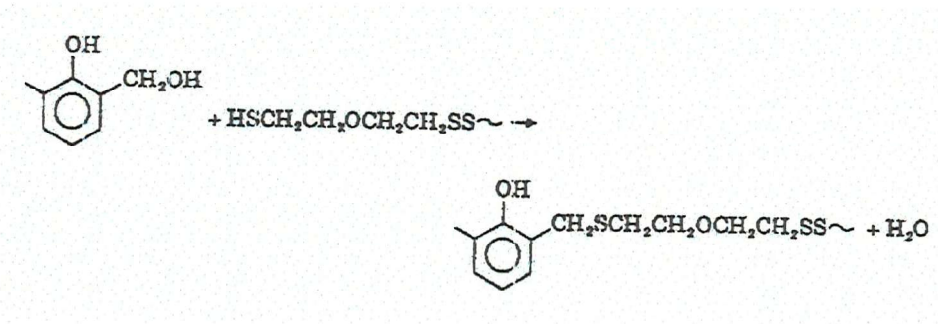


Other additives commonly found in sealants are:

- Pigments used so that the adhesive's colour is similar to that of the adherend.
- Wetting agents are added so that the adherend faces are wetted sufficiently for good adhesion.
- Reactive diluents of low-molecular weight; compounds containing reactive groups, used to reduce the viscosity of adhesives.
- Extenders are inexpensive materials added so that the cost of adhesives is minimised.
- Inhibitors that retard the curing process so as to extend both the working and shelf lives of the adhesive.

**The Curing Agent :** The three most commonly used curing agents are dichromates such as $CaCr_2O_7$ and $MgCr_2O_7$, manganese dioxide, a base catalysed cure, and, epoxy resins. An accelerator is usually included such as diphenylguanidine [8]. Recently environmental considerations have become important regarding the use of chromates as curing agents. Sodium stearate is often included with the curing agents in order to offset the effect of diphenylguanidine and to allow minor adjustment to the cure rate and application time.

Other components of the curing agent would be suitable fillers, volatiles such as toluene and methyl ethyl ketone and, hydrogenated terphenyls as a dispersing oil .

The liquid polysulfides are cured to elastomeric solids by oxidation of the thiol terminal groups. The cure reaction can be generally represented as follows [1]:

$$X(\text{HS-(R-SS-)}_n\text{-R-SH}) + [O] \rightarrow (\text{-S-(RSS)}_n\text{-R-S-})_x + H_2O + \text{reduced products}$$

The process of oxidation of the terminal thiol groups results in the production of polymer chains of large molecular weight.

Crosslinked rubbers do not dissolve in solvents unless the structure disintegrates. Instead the polymers swell with the resistance to swelling depending on the solvent and the cross-link density of the polymer. Interaction between the rubber and the solvent causes the polymer chains to push apart as the solvent is soaked up. This continues until the internal stresses of the polymer structure are too great, preventing any further swelling.

### 3.1.4 Solubility Parameter

Hilderbrand and Scott defined a solubility parameter, $\delta$, such that

$$\delta^2 = E/V$$

where E is the energy of vaporisation and V is the molar volume.
In the absence of hydrogen bonding, it was shown that

$$\Delta H = V_m(\delta_1 - \delta_2)^2 \Phi_1 \Phi_2$$

where $V_m$ is the total volume of the mixture, $\delta_1$ and $\delta_2$ are the solubility parameters and $\Phi_1$ and $\Phi_2$ are the molar volume fractions. The subscripts 1 and 2 represent the solvent and polymer respectively. $\Delta H$ will approach zero as $\delta_1$ approaches the value of $\delta_2$.
In general, rubbers swell most in a solvent with a similar solubility parameter. Aviation fuel, which is predominantly aliphatic hydrocarbons of low $\delta$, would be only

expected to swell polysulfides (which have a solubility parameter of ~9.3 Hildebrands) to a low extent.

### 3.1.5 Theories of Adhesion

There are several definitions of the term 'adhesion'. Adhesion can be termed the bond formation between a solid surface and a second liquid or solid phase. Theories on the mechanism of adhesion can be divided into the following categories:

*a.* **The diffusion theory of adhesion,** which refers to adhesion between two polymers, suggests that the bond and bond strength is a result of the diffusion of polymers across the interface [10]. According to this theory, adhesion of two polymers results from the interdiffusion of molecules from the surface layers of the polymers. An interphase is formed between the two polymers [11]. For adhesion by interdiffusion to occur the polymers must be soluble in each other and at a temperature high enough to permit the polymers' mobility.

This theory is limited to autohesion (diffusion of identical molecules) and adhesion of compatible polymers.

*b.* **Mechanical adhesion** In this method the surfaces undergoing adhesion interlock on a microscopic scale [12,13]. It is the mechanical interlocking of the polymer into the pores and other irregularities of the adherend surface, which results in adhesion. The anodised surface of aluminium is a good example where the adherend provides sites for interlocking. The oxide surface consists of hexagonal structures with an approximately circular pore through the centre of each [14]. The adhesive polymer flows into the pores through capillary action and then sets, resulting in adhesion [15]. Work by Packam has shown that polyethylene must be oxidised in order to produce good adhesion with aluminium oxide surfaces without pores, while aluminium oxide surfaces with pores produced good adhesion in the absence of oxidation of the polyethylene [16,17]. In fact the bond strength was directly proportional to the depth of the pores and the overall porosity

of the oxide surface. A study by Venables et al [18] of the standard treatment used in the adhesive bonding associated with aerospace applications has shown that the pore and whisker formation produced by chromic etching and subsequent phosphoric acid anodisation, results in a bond which only fractures upon cohesive failure. Without the pore and whisker structure the failure occurs at lower peel strengths. It should be remembered that the adhesive has to wet the surface. The wetting process is described in section 3.1.6.

*c.* **The electrical theory of adhesion.** This theory proposes that an electrical double layer is formed at the interface due to the attractive electrical forces between the adherend and adhesive [19]. Deryagin and Krotova have suggested that the two surfaces produce a capacitor-like structure with the energy of adhesion equal to the energy of separation of the two capacitor faces [20]:

$$W = \frac{\delta^2 h}{2\varepsilon}$$

where δ is the surface charge density, h is the distance between the charge planes, and ε is the dielectric constant of the medium. *In-situ* evidence for the electrical double layer was produced by Possart for the case of an aluminium-low density polyethylene assembly [21]. He also proved that the contribution towards the overall adhesive strength was small.

*d.* **The adsorption theory** suggests that adhesion occurs due to a combination of hydrogen bond, dipole-dipole, London dispersion forces and the surface free energies of the adhering materials [22,23]. Thus, the theory describes the physical bonds that may exist between the substrate and the adhesive. Also included in the theory are Lewis acid-base interactions which results in the following equation for the work of adhesion ($W_a$) [22].

$$W_a = W_a^{phys} + W_a^{chem}$$

Where $W_a^{phys}$ is the sum of the physical interactions and $W_a^{chem}$ includes hydrogen bonding and the Lewis acid-base interactions.

The physical forces are only significant over a distance of a few Ångströms. Therefore, extremely close contact and complete wetting are required for adhesion.

*e.* **The chemical adhesion theory** proposes that chemical bonding results in adhesion. The adhesion by chemical bonding only involves a small number of molecules [19]. The chemical bond may occur in bridging mechanisms where a molecule, for example silanes, reactive at both ends bonds two materials together. Adhesion involving chemical bonding is commonly observed in the case of polymer-metal interfaces where generally covalent bonds are formed between the polymer and the metal surface.

None of the above theories completely explain adhesion and only a combination of a collection of them will ever result in a general theory of adhesion.

### 3.1.6 Wetting

Thomas Young studied the equilibrium state of a drop on a surface. He proposed the following equation to describe the relationship between surface tension and contact angle:

$$\gamma_{SV} = \gamma_{SL} + \gamma_{LV} \cos\theta_{SL}$$

where $\gamma_{SV}$ = surface energy of solid in contact with liquid vapour, $\gamma_{LV} = \gamma_L$ = surface energy (or tension) of liquid in contact with its vapour, $\gamma_{SL}$ = interfacial solid-liquid energy and, $\theta_{SL}$ = contact angle of liquid against solid.

Dupré proposed the following equation for the thermodynamic work of adhesion:

$$W_{SL} = \gamma_S + \gamma_L - \gamma_{SL}$$

Thus the thermodynamic work of adhesion of a liquid to a solid is given by the sum of the surface free energies of the individual solid and liquid phases minus the interfacial free energy. In a paper by Driver the spreading pressure, $\Pi$, is defined as $\gamma_S - \gamma_{SL}$, and taking this into account the Young-Dupré equation results [24]:-

$$\gamma_S = \gamma_{SL} + \gamma_{LV}\cos\theta_{SL} + \Pi$$

Hence,

$$W_{SL} = \gamma_L (1 + \cos\theta_{SL}) + \Pi$$

Now, the cohesive energy of a liquid is given by:

$$W_{LL} = 2\gamma_L$$

For a liquid to completely wet a solid the contact angle must be equal to zero. Hence it is obvious that the condition for total wettability is:

$$W_{SL} \geq W_{LL}$$

When the energy of adhesion is greater than or equal to the cohesive energy of the liquid total wetting is achieved.

### 3.1.7 Pretreatment of surfaces

Layers of contamination on matter are encountered as shown in Figure 3.1:

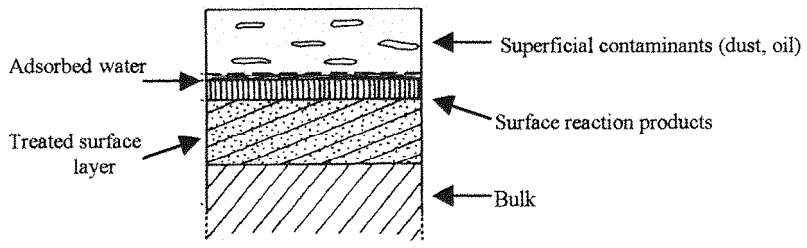

The natural surface layers usually should be removed prior to bonding as they provide a weak surface for bonding which is incompatible with the polymer.

The purpose of surface pretreatments is to generate a well-defined and active surface with an affinity for the coating considered. The surface energy $\gamma$ of the new surface must also be sufficient so that the applied adhesive or coating can wet or spread out. This condition is fulfilled when $\gamma_{solid} \geq \gamma_{liquid}$. The surface energy of the solid may thus be increased by treating the surface of the solid. There are various methods for treatment which are listed as follows:

1. Mechanical : abrasion, sand blasting
2. Solvent degreasing: using the condensation of the vapour.
3. Chemical:
   - Chromic or sulphochromic oxidation – This involves the use of $H_2SO_4/CrO_3/H_2O$ producing an oxide layer with a cellular structure on the surface of the aluminium. The thickness of the layer is usually < 15 nm.
   - Anodisation – This is an electrochemical process using either a sulphuric, chromic or phosphoric electrolyte. The aluminium acts as the anode reacting with the oxygen produced and forming an anhydrous $Al_2O_3$ oxide layer approximately 15 to 20 μm thick [19]. This layer is partially dissolved by the electrolyte resulting in the formation of numerous hexagonal cells with a pore in the middle of each.
   - Phosphatization – The aluminium surface is treated with a solution of phosphoric acid, chromic acid and a fluoride catalyst producing a phosphates layer. This layer is assumed to have the following composition: $Al_2O_3$, $2CrPO_4$, $8H_2O$. The dry coating is essentially composed of $Cr^{III}$ and aluminium phosphates [25].
4. Physico-Chemical: flame, corona discharge, cold plasma
5. Application of adhesion promoters or primers

### 3.1.8 Adhesion Promoters

An adhesion promoter is a coupling agent that improves adhesion by promoting stronger interfacial interactions between the adhesive and the substrate. The most common examples of adhesion promoters are organosilanes, typically of the formulation: R'-Si-$(OR)_3$ where R' is a reactive group such as epoxy and (OR) is an alkoxy group (see Figure 3.2) [26]. The silane end is hydrolysed in the presence of water and will form strong chemical bonds with metal or glass. The organic (epoxy) end encourages bonding with polymers.

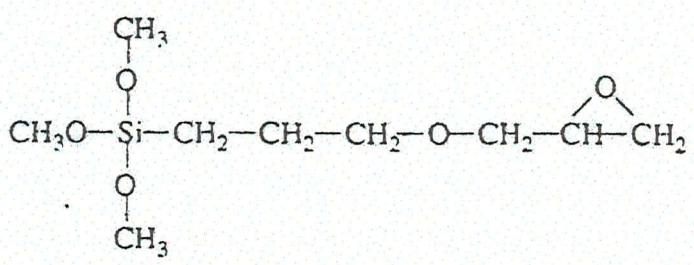

**Figure 3.2 :** *An example of an organosilane adhesion promoter*

Other types of adhesion promoter are the organic titanates which have the general structure:

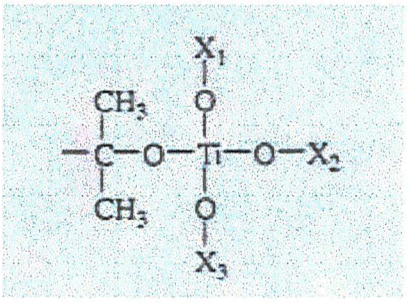

Where $X_1$, $X_2$ and $X_3$ are organic substituents such as epoxies.

Often the adhesion promoter is added to the base polymer adhesive and thus promotes bonding before the adhesive has cured [27-28].

### 3.1.9 Primers

The importance of using primers for the pre-treatment of the surfaces to be adhesively bonded has gradually emerged. Primers are usually dilute solutions containing a coupling agent. Currently the most popular primers are epoxy paints that are sprayed onto the anodised surface before the adhesive is applied. Primers are used in a bonding system for one or more of the following functions [29]:

*a.* Protection of the surface of the adherend.
*b.* Greater wettability with respect to subsequent coating.
*c.* Improvement of the surface interaction (solubility) between adhesive and adherend
*d.* Promotion of chemical and physical reactions between adhesive-primer and adherend-primer interfaces.

Most metals can be processed without priming, at least, if the adhesive is applied to the freshly etched surface within a few hours. However, fatigue properties (material failure due to cyclic stressing) and moisture resistance of bonded metal surfaces in the aircraft industry are improved by suitable primers. The primed metal surface should be completely free of all dirt and grease for good adhesion and this is usually achieved by solvent-wiping the surface prior to application of the sealant. However it is shown in this work that this is totally ineffective and the use of an adhesion promoter is necessary.

The production of bonded structures can therefore be split up into two separate processes:

*a.* The preparation of the metal surfaces.
*b.* The application of the adhesive and the adhesive curing.

The adhesive strength results from the adhesive properties of the resin and those of the specially treated metal surfaces. The cohesive strength is the result of the curing process and deals with the strength of the actual adhesive material. Fracture at the interface between the adherend and the adhesive is known as ***adhesive failure***. The separation of the adhesive from itself is known as ***cohesive failure***.

## 3.2 Experimental Procedures

### 3.2.1 Techniques

Microtoming: This is a method of cutting samples to a required thickness. The sample is fixed to a stage and is then cut into thin slices using a glass knife. The glass knife is made with a very fine cutting edge so that a smooth cut is produced. The knife is pulled manually, at an approximately constant rate, over the surface of the sample producing the desired slices. Height adjustment moves the knife-edge up and down through several microns with regard to the surface of the sample.

Specular and ATR FT-IR: Both of these methods have been described in **Chapter 2.** The ATR crystal used zinc selenide which has a refractive index of 2.4.

### 3.2.2 Procedures

It was decided on discussion with BAe that only the fillet sealant should be examined and in particular the fillet sealant PR1422 B2, a dichromate cured system, although samples of MC238 sealant, a manganese cured system, were also supplied. To begin the sealant samples were all received as peel-tested samples. They all consisted of an aluminium substrate measuring 150*70*1 mm. The aluminium was anodised and then sprayed with an epoxy primer paint. A variety of primer paints were used. These were PR205, PR143 and AKZO 37035A, the most common being PR143. The painted surface was cured for 2 hrs at 50 °C. Afterwards the surface was abraded, using a light grade of sandpaper, or not abraded depending on the choice of sealant. All work presented here considers the use of PR1422 B2 and abrasion of the surface was undertaken. The surface was then solvent wiped using Purasolv (ethyl lactate) and air-dried. Two strips of sealant (~25 mm across) were applied to each substrate. The sealant was applied to a total thickness of ~4.5 mm and wire mesh was placed in the sealant ~3.0 mm above the substrate, (refer to Figure 4.2.2).

### 3.2.2.1 FT-IR reflectance spectra of the primer painted surface

Suitably sized pieces of the primer painted Al substrate were placed in the specular reflectance apparatus and the reflectance spectra of the surfaces recorded on a Perkin-Elmer 1700 series IR spectrometer. All spectra were corrected for background, recorded at room temperature with dry air being flushed through the spectrometer. Usually 25 scans were recorded. The spectra, which resembled first derivatives, were then analysed using the Kramers-Kronig function on the IRDM programme, and converted into transmission-like spectra.

### 3.2.2.2 Microtoming of sealant samples

A sample of sealant PR1422 B2 measuring ~20 $mm^2$ was placed on a piece of wetted tissue paper and placed upon the stage of the microtome. The stage was cooled electrically to ~(-20 °C), at which temperature the sealant was 'frozen' onto the stage. Once the temperature had reached an equilibrium, slices of sealant were cut from the sample using the glass knife by sweeping it over the sample. Adjustment of the knife-edge determined the thickness of slice cut. Usually a few thick slices were cut exposing the interior of the sealant before slices ~10 μm in thickness were taken.

### 3.2.2.3 ATR study of the PR1422 B2 sealant 'slices'

The microtomed sealant slices were placed on the ATR crystal surface. The ATR apparatus was then mounted in a Perkin-Elmer 1700 series IR spectrometer. Adjustment of the ATR apparatus was undertaken until the maximum energy of transmission was achieved. The ATR spectrum of the microtomed sealant was recorded. Also recorded was an ATR spectrum of sealant sample, which had not been microtomed. All spectra were corrected for background, recorded at room temperature with dry air being flushed through the spectrometer.

#### 3.2.2.4 Raman study of the sealant

A specimen of sealant was placed in a sample holder and placed in the sample compartment of a Perkin-Elmer 1700 series Raman spectrometer. The power of the laser was reduced to a sufficiently low level so that, it was hoped, burning of the sealant would not occur.

#### 3.2.2.5 Study of the effectiveness of Purasolv in removing all traces of cetyl alcohol

The surface of the ATR crystal was coated with cetyl alcohol solution (12.01g of cetyl alcohol in 100 ml of white spirit at 54 °C). The crystal and sample coating were left to cool for two hours before an ATR spectrum was recorded. Consecutive ATR spectra were recorded after successive solvent wiping (using Purasolv) of the cetyl alcohol coated crystal surface until a total of 10 wipes had been completed.

#### 3.2.2.6 Gravimetric study of the affects on the sealant due to exposure to aviation fuel

Weighed samples of sealants PR1422 B2 were exposed to fuel, at room temperature, for 7, 14, and 28 day periods. The aviation fuel used was a synthetic version consisting of 2,2,4-trimethyl pentane (30% v/v) and toluene (70% v/v). The exposed samples were weighed to gravimetrically analyse the amount of fuel take-up by the sealant. They were then left exposed to air until there was no significant mass change and again their masses were recorded.

#### 3.2.2.7 Gravimetric study of the affects on the sealant due to exposure to distilled water

Weighed samples of the sealants PR1422 B2 were exposed to distilled water, at room temperature, for 7, 14 and 28 day periods. The exposed samples were weighed to gravimetrically analyse the amount of water take-up by the sealant. They were then left exposed to air until there was no significant mass change and again their masses were recorded.

### 3.2.2.8 Study of 'old-wing' specimen to determine the mode of sealant failure and possible cause

A sample of deteriorated sealant, (PR1422 B2), from an old wing specimen from an aeroplane no longer in service was provided by BAe. This was examined both visually and under a microscope to determine whether the failure of the sealant was due to adhesive or cohesive failure. This sealant would have been exposed to all of the possible conditions that would be expected during its service life.

## 3.3 Results and Discussion

### 3.3.1 Infrared study of primer painted surfaces

Using an infrared specular reflectance accessory it was possible to record reflectance spectra of the primer paints. These spectra resemble a first derivative spectrum. Using the Kramers-Kronig application the spectra were converted to resemble transmission spectra. The primer painted surfaces produced the following spectra:

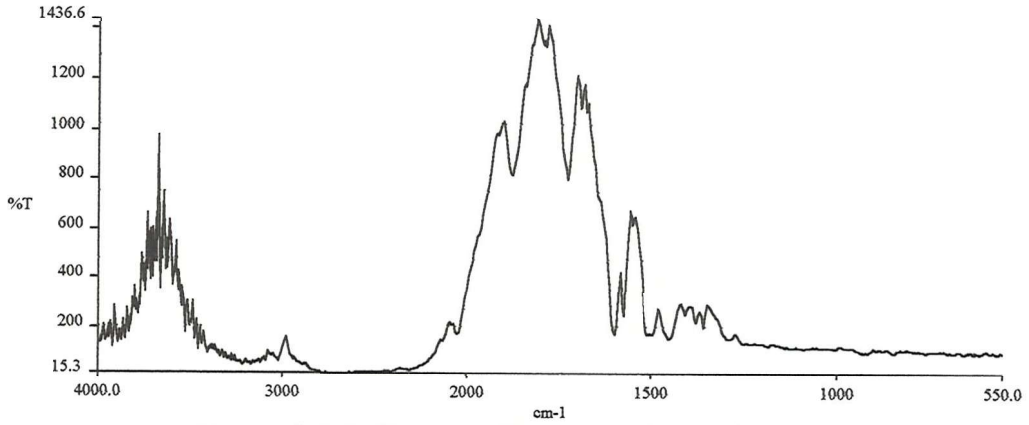


***Figure 3.3.1:*** *Kramers-Kronig analysis of specular reflectance spectrum of PR143 primer paint*

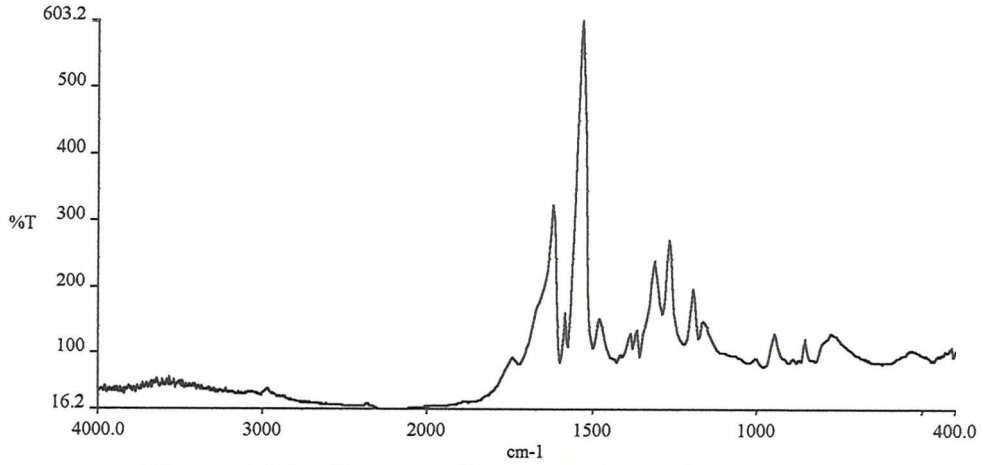


***Figure 3.3.2*** *: Kramers-Kronig analysis of specular reflectance spectrum of AKZO 37035A primer paint*

The only information supplied regarding the paints was that they contained epoxy groups with leachable, soluble chromates. Understanding that it is the epoxy that

promotes bonding to the sealant it was decided that no in-depth assignment of the bands in the paints spectra was required at this point. The surfaces were to be examined again after testing.

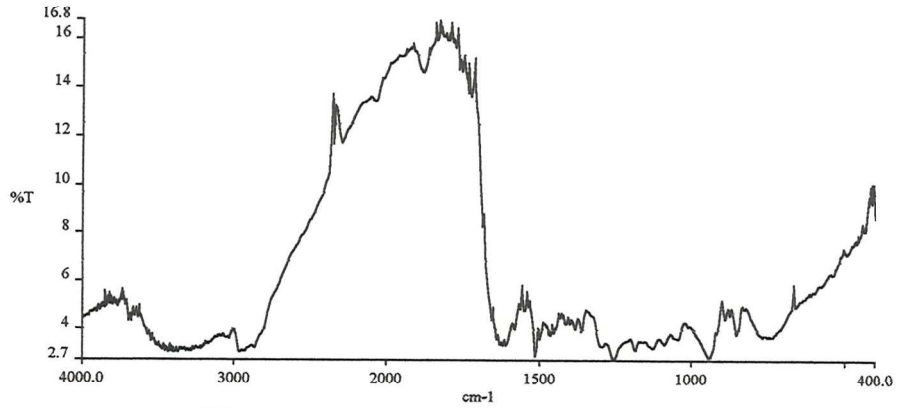


***Figure 3.3.3*** *: Kramers-Kronig analysis of specular reflectance spectrum of PR205 primer paint*

Sealant samples were bonded to these paints and left to deteriorate. These spectra were recorded in order that comparison may be made with spectra of the surfaces, recorded after a sealant has undergone failure, to determine whether cohesive or adhesive failure has occurred.

### 3.3.2 Microtoming of sealant samples

The slices microtomed from the sealant PR1422 B2 were of the order of 10 μm thick. It was found that as expected the colder the temperature of the stage the 'cleaner' the slices i.e. less rippling of the slice. Microtoming is a cumbersome and time-consuming process to the amateur but, however, the only method to produce thin regular slices of the sealant known to this student. With practice, this process produced some thin slices of the sealant but however transmission infrared spectra were of poor quality as compared to those attained using the ATR technique (Figures 3.3.4 and 3.3.5). It was decided that is was not necessary to produce transmission spectra as study using an ATR crystal was simpler and more convenient.

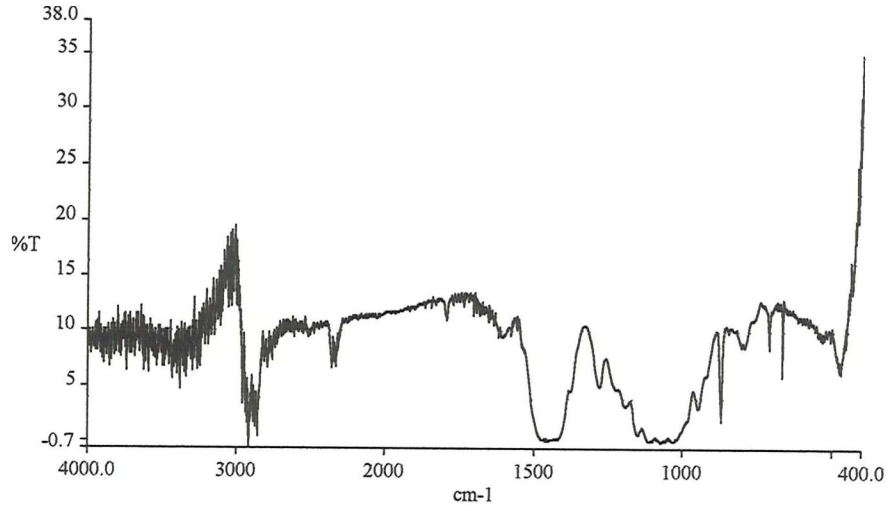


***Figure 3.3.4**: Transmission spectrum of microtomed sealant PR1422 B2. (Resolution 1 $cm^{-1}$)*

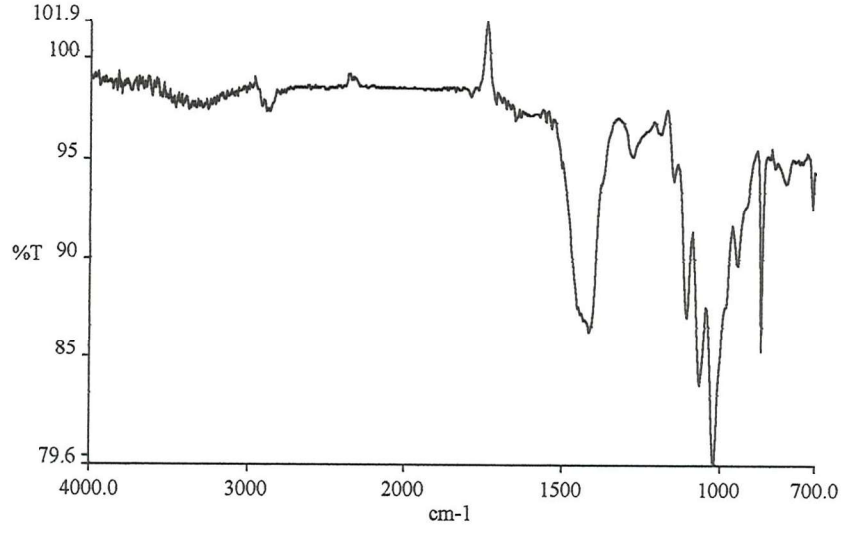


***Figure 3.3.5**: ATR Spectrum of microtomed sealant PR1422 B2. (Resolution 4 $cm^{-1}$)*

### 3.3.3 ATR study of the sealant PR1422B2

The absorption bands of the S-H, C-S and S-S vibrations of organic sulfur compounds are of very low intensity. The S-H stretching vibrations are found between 2600 $cm^{-1}$ and 2250 $cm^{-1}$. The asymmetric and symmetric C-S-C stretching vibrations occur between 1030-800 $cm^{-1}$ and, 1220-1060 $cm^{-1}$, respectively. The S-C stretching vibration absorbs at 750-600 $cm^{-1}$. The C-S-C bend occurs between 715 and 660 $cm^{-1}$. The S-S vibrations are found at 550-450 $cm^{-1}$.

The S-H stretching vibrations are not found in the following spectra. This is probably due to the fact that the spectra are recorded for cured sealant and therefore there are relatively few S-H groups (1-2% thiol content) [8]. Also the lowest wavenumber

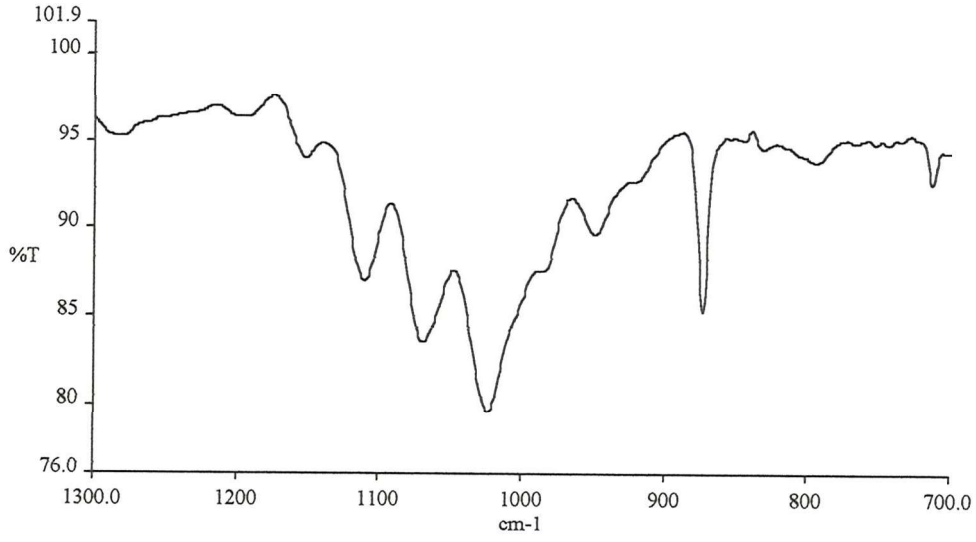


***Figure 3.3.6** : ATR spectrum of sealant PR1422 B2 recorded between 1300 – 700 $cm^{-1}$*

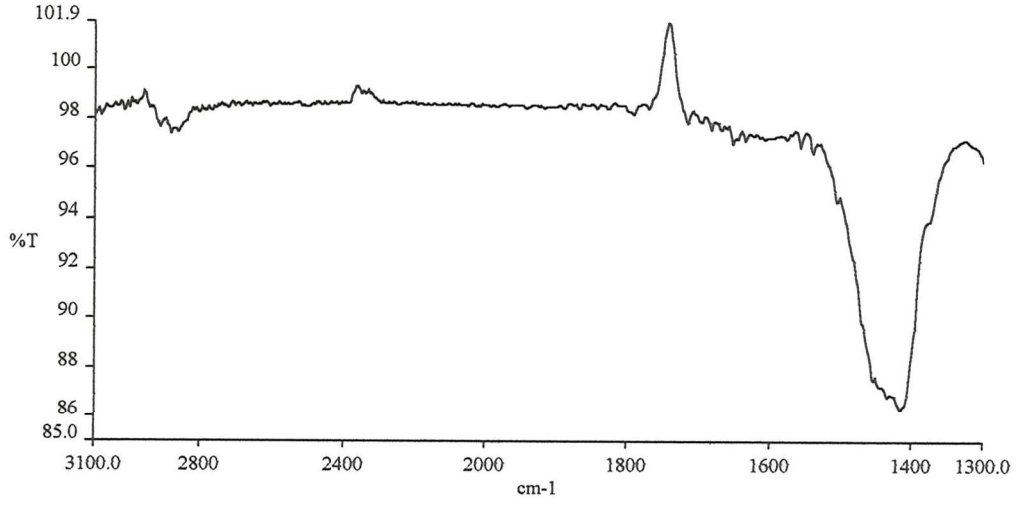


***Figure 3.3.7** : ATR spectrum of sealant PR1422 B2 recorded between 3100 – 1300 $cm^{-1}$*

measured is 600 $cm^{-1}$ as the ATR zinc selenide crystal does not transmit below 16 μm. Therefore, it has not been possible to identify the presence of S-S vibrations.

Peaks found in these spectra (Figs.3.3.6-7) could correspond to the following:

| **Peak position ($cm^{-1}$)** | Vibration |
|---|---|
| 712 $cm^{-1}$ | -C-S-C- bend |
| 794 $cm^{-1}$ | -C-H bend |
| 873 $cm^{-1}$ | -C-O-C- sym. stretch, C-H bend *or* epoxide |
| 949 $cm^{-1}$ | -C-O-C- sym. stretch |
| 1069 $cm^{-1}$ | -C-O-C- sym. stretch |
| 1109 $cm^{-1}$ | -C-O-C- asym. stretch |
| 1280 $cm^{-1}$ | -C-O-C- asym. stretch |
| 1260-1240 $cm^{-1}$ | $-H_2C$-CH-R <br> O |
| 1417 $cm^{-1}$ | -C=C-H bend, $-CH_2$ bend *or* $-S-CH_2-$ (C-H) stretch/bend |
| 1793 $cm^{-1}$ | -O-C-O- |
| 2885 $cm^{-1}$ | -C-H sym. stretch |

***Table 3.3.1:*** *Assignments of bands found in spectra of sealant PR1422 B2*

### 3.3.4 Raman study of the sealant

Attempts to study the sealant using Raman spectroscopy have all proved to be futile at this stage. Figure 3.3.8 shows the spectrum produced which is the typical spectrum of

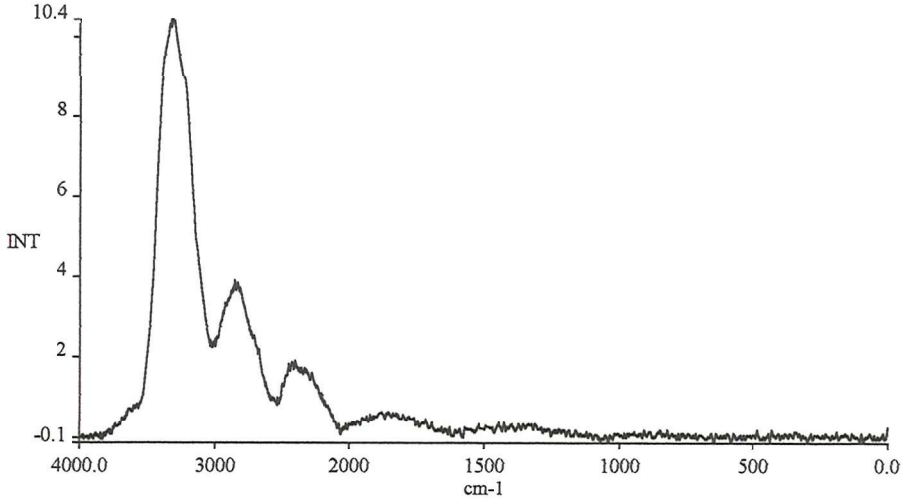


***Figure 3.3.8*** *: Raman spectrum of polymer clearly showing that the laser is burning the polymer*

a burning sample. Burning of the sealant occurred at very low laser power, with the fumes of sulfur dioxide being pungently evident. Thus, no Raman spectrum of the sealant has been recorded. The use of freshly cleaned KBr discs in an attempt to dissipate the heat of the laser proved unproductive. Using Al powder mixed in with the sealant to try to dissipate some of the heat also failed. A method by which the spectra could be recorded in the future would be by rotating the sample. This would prevent any one point in the sample becoming hot enough to burn.

### 3.3.5 Study of the effectiveness of Purasolv in removing all traces of cetyl alcohol

As can be seen from Figure 3.3.9 the solvent cleaner Purasolv does not completely remove all traces of cetyl alcohol, ($C_{16}H_{33}OH$), from the surface. The general practice at BAe is to simply wipe the surface of the primer painted metal once with Purasolv in the belief that this completely cleans it. However, the evidence presented here proves that the surface is not nearly completely cleaned and thus any problems that the presence of cetyl alcohol will have on adhesion will have to be investigated. It is not being very speculative to assume that the presence of cetyl alcohol on the painted surface is detrimental to proper adhesion of the sealant.

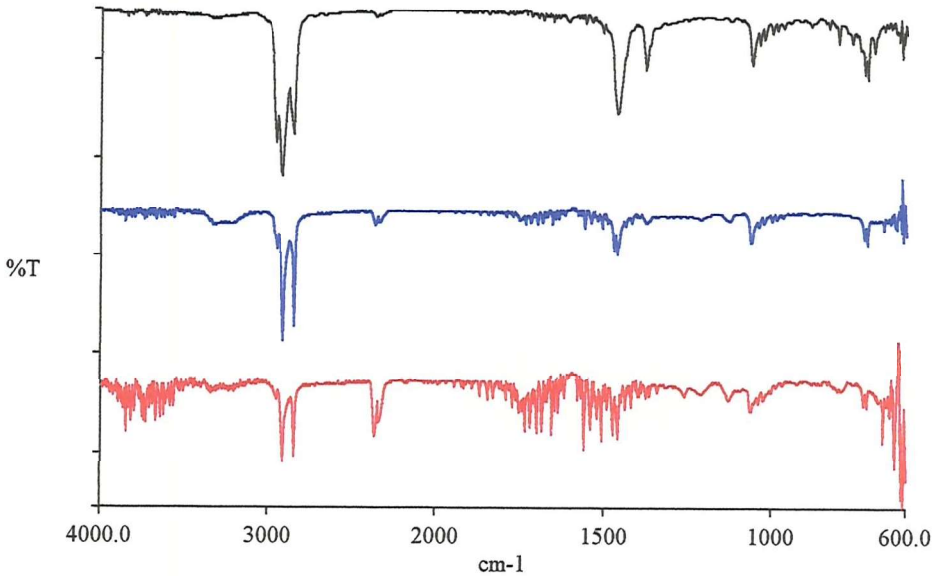


***Figure 3.3.9 :*** *ATR spectrum of cetyl alcohol coating, after wiping with Purasolv solvent - 1 wipe, - 3 wipes and, - 10 wipes*

### 3.3.6 Gravimetric study of the affects on the sealant due to exposure to aviation fuel

The amount of fuel that is taken up by the sealants PR1422 B2 was found to be in the region of 5% by mass of the sealant. The sealant samples returned to within 1% of their original masses within 7 days. Thus, the sealant may swell and shrink slightly as it is exposed to fuel. The adhesive properties of the sealant would be subject to strains and stresses and over a period of time sealant deterioration will occur. Therefore, studies of how the properties of the sealant change over time under fuel exposure, and how to improve the resistance of the sealant to fuel take-up have to be undertaken. The main problems possibly lie with leaching of the materials from the sealant and possible diffusion of solutes occurring. This is investigated in chapter 4.

| Time (days) | Mass of sample (g) | % Mass change |
|---|---|---|
| 0 | 23.56 | |
| 7 | 24.29 | 3 |
| 14 | 24.57 | 4 |
| 28 | 24.68 | 4 |

***Table 3.3.2 :*** *Fuel absorption of PR1422 B2*

### 3.3.7 Gravimetric study of the affects on the sealant due to exposure to distilled water

The amount of water that is taken up by the sealant PR1422 B2 is of the order of 20 % by mass of the sealant. Researchers at the Sowerby Research Centre have shown that the amount of water uptake to be of the order of 200 % by mass for some sealants [30]. This must have disastrous affects on the adhesive properties of the sealant and these affects must be investigated. They have shown that after exposure to water a manganese-cured sealant (MC238) becomes sponge-like and breaks up extremely easily. The actual rate of take-up and its dependence on temperature are not yet

known. The temperature in the fuel tanks can reach over 80 °C on runways in tropical countries. The affect of this on the sealant has to be examined.

| Time (days) | Mass of sample (g) | % Mass change |
|---|---|---|
| 0 | 24.44 | |
| 7 | 27.07 | 10 |
| 14 | 28.21 | 15 |
| 28 | 28.99 | 18 |

***Table 3.3.3 :*** *Water absorption of PR1422 B2*

### 3.3.8 Study of 'old-wing' specimen to determine the mode of sealant failure and possible cause

Under the microscope it was revealed that in fact a thin layer of adhesive sealant was present on the old-wing specimen samples where sealant failure had occurred. Thus, it is cohesive failure that has occurred during the lifetime of the aircraft and there is no difficulty with the adhesion between the primer paint and the adhesive sealant. Accordingly, the problem lies with the adhesive. The effects that chemical and environmental exposure have on the sealant are examined in Chapter 4.

## 3.4 Conclusions

Introduction to the chemistry and theories of polysulfide sealants has been presented. Specular reflectance spectra have been recorded for the primer paints that are currently being used by British Aerospace. These served the purpose of reference spectra so that once a sample had been peel-tested, (see Chapter 4) and, the mode of failure was difficult to determine, comparison of reflectance spectra would reveal whether cohesive or adhesive failure had occurred.

ATR spectra have been recorded for the dichromate cured sealant PR1422 B2. The peaks have been tentatively assigned. Peaks for the thiol groups did not appear in the spectra possibly as a result of the polymer being cured and a thiol content of 1-2 % [8].

ATR spectroscopy also revealed that the method of solvent wiping the painted surfaces to remove cutting fluid (cetyl alcohol) was completely ineffective.

Raman spectroscopy failed to produce a spectrum due to burning of the sealant sample.

## References:


1. R.E. Meyer, *SAMPE Journal*, **18**, 6, (1982).
2. A.A. Duell, *Surface Coatings*, **1**, 1, (1965).
3. A.M. Usmani, *Polymer News*, **10**, 8, (1985).
4. BAe report, No. 2212/05XR/MAT, April 1988.
5. S.K. Flanders, *Modern Paint and Coatigs*, **79**, 6, (1989).
6. H. Singh, *Rubber World*, **19**, 5, (1987).
7. N.D. Ghatge, S.P. Vernekar, S.V. Lonikar, *Rubber Chemistry and Technology*, 54, (1980).
8. B.C. Ennis, P.J. Hanhela, R.H.E. Huang, G.J. Long, D.B. Paul, *Journal of Applied Polymer Science*, **41**, 11-12, (1990).
9. M.B. Berenbaum, J.R. Panek, in *Polyethers, Part III, V.*, N.G. Gaylord Ed., (Interscience Publishers, New York), pp 43- 224.
10. S.S. Voyutskii, Y.L. Margolina, *Rubber Chem. Technol.*, **30**, 531, (1957).
11. L.H. Sharpe, *Polym.Prepr. (Am.Chem.Soc.Div.Poly.Chem.)*, **37**, 2, (1996).
12. D.E. Packham, *Journal of Adhesion*, **39**, 2-3, (1992).
13. K.W. Allen, *Int.J.Adhesion and Adhesives*, **13**, 2, (1993).
14. K. Bright, B.W. Malpass, D.E. Packham, *Br. Polym. J.*, **3**, 205, (1971).
15. V.V. Arslanov, V.A. Ogarev, *Kolloid Zh.*, **39**, 934, (1977).
16. D.E. Packam, K. Bright, B.W.Malpass, *J.Polym.Sci.*, **18**, (1974).
17. D.E. Packam, in *Aspects of Adhesion 7*, edited by D.J. Alner and K.W. Allen, (Transcripta Books, London, 1973), pp 51-63.
18. J.D. Venables, *J. Mater. Sci.*, **19**, 2431, (1982).
19. G. Fourche, *Polymer Engineering and Science*, **35**, 12, (1995).
20. B.V. Deryagin, N.A. Krotova, *Dokl. Akad. Nauk. SSSR*, **61**, 849, (1948).
21. W. Possart, *Int. J. Adhes. Adhes.*, **8** (2), 77, (1988).
22. J.C. Berg, *Nordic Pulp and Paper Research Journal*, **8**, 1, (1993).
23. L.H. Sharpe, H. Schornhorn, *Chem. Eng. News.*, **56**, 40, (1964).
24. D. Driver, *High Performance Materials for Aerospace*, Chpt 11, (1995).
25. L.A. Nimon, G.K. Korpi, *Plating*, **59**, 421, (1972).
26. M.N. Sathyanarayana, M. Yaseen, *Progress in Organic Coatings*, **26**, 2-4, (1995).

**27.** R. Ramaswamy, P.S. Achary, *Org.Coat.Appl.Polym.Sci.Proc.*, **47**, (1982).

**28.** S.S. Mahajan, N.D. Ghatge, *Intern.J.Polymeric Materials*, **10**, 2, (1983).

**29.** D.M. Brewis, G.W. Critchlow, *Trans. Inst. Met. Finish*, **74**, 6, (1996).

**30.** BAe Report, No. JS. 13398, January 1996.

# Chapter 4

# Analysis of the Sealant PR1422 B2

# Chapter 4

# Analysis of the sealant PR1422 B2

## 4.1 Introduction

This chapter focuses on the degradation of polymers, more specifically the sealant PR1422 B2, as studied by analytical methods such as infrared and Raman spectroscopies. The use of spectroscopy to study the degradation is outlined using examples from a wide range of applications before a more detailed discussion regarding the sealant. Degradation is the result of undesirable changes in properties when the polymer is in use. Decomposition of a material through physical means such as weathering, or by chemical means, for example, ozone attack may occur. Degradation does not always result in complete destruction of a material. A sealant may lose some of the adhesive properties or disintegrate as a result of degradation. Degradation can occur in loss of oligomers or additives including fillers or plasticisers. Sealants can therefore leak due to the degradation process and either have to be repaired or replaced, in both cases at great expense for the aircraft industry.

### 4.1.1 The study of degradation

Various analytical techniques exist which may be used to study polymer degradation and the area where adhesive or cohesive fracture between the sealant and substrate occurs. The surface of the polymer and/or the substrate after degradation can be studied using the following techniques [1,2]. Auger electron spectroscopy is used to quantitatively analyse the elements present. X-ray photoemission spectroscopy and UV photoemission spectroscopy are used to gain information on the electronic structure. Electron energy loss spectroscopy is used both to analyse the electronic and vibrational structures. The two microscopy techniques, scanning tunnelling microscopy and atomic force microscopy reveal information on the surface topography.

A technique used to study the polymer degradation process would be the thermo gravimetric analysis-infrared procedure (TGA-IR). In a paper by Wilkie and

Mittleman, TGA-IR was used to study Nafion-H, (a tetrafluoroethylene backbone with sulfonic acid groups), and poly (2-sulfoethyl methacrylate) and methyl methacrylate copolymers [3]. As the polymer is heated and thus degrades the infrared spectrum reveals the products given off and the gravimetric analysis reveals the percentage of each product.

### 4.1.2 Uses of IR spectroscopy and Raman spectroscopy to study degradation

Infrared spectroscopy and Raman spectroscopy have been widely used in analytical fields to study degradation. A paper by Owen [4] discusses the use of infrared spectroscopy to study the chemical effects of weathering in trees. The wood was examined by diffuse reflectance infrared spectroscopy after varying degrees of light and water exposure. Owen relates the spectral changes, which occur after the wood has been exposed to light for only 300 hours. The woods chosen were microtomed slices (10 μm) of western redcedar and southern pine. The polymer composition of each tree is unique and therefore produces a characteristic spectrum. After weathering it was noted that the intensity of the peaks at 1600 $cm^{-1}$ and 1510 $cm^{-1}$ arising from the aromatic rings of lignin decreased, and a carbonyl peak at 1750 $cm^{-1}$ displayed an increase in intensity [4]. These, according to Owen, relate to the bond breaking and free radical formation associated with exposure to UV. Water exposure leached out the polymer fragments rich in carbonyls resulting in a corresponding decrease in the peak at 1750 $cm^{-1}$.

Another example would be a study of oil paints where laser Raman spectroscopy was used to study curing and degradation [5]. The oil paints studied were ZnO White and $TiO_2$ White and at a film thickness of 0.2 mm. The paints were exposed to irradiation by a Xe lamp. The curing of the paints was studied by observing the disappearance of the spectral evidence for C=C bonds. The degradation, by Xe irradiation, was proposed to occur via the formation of carbonyl compounds, which were evident in the spectra [5]. Thus, being able to study and understand the degradation process provides a route to improving oil paints.

An area where much research has been carried out is the degradation of rubbers under ozone exposure [6,7]. Ozone oxidises both unsaturated and saturated organic polymers.

S.G.Hong discusses the case where polymers are subjected to a stress the ozonolysis reaction can occur more rapidly [8]. He studied the effect ozone exposure and applied stress to ethlyene-propylene-diene terpolymer in a polypropylene matrix. In the paper ATR infrared spectroscopy is used to follow the degradation process by recording the formation of new bands in the spectra near 1746 $cm^{-1}$ and 1714 $cm^{-1}$, characteristic of carboxyl and carbonyl groups typical of degradation products. Also a new peak at 1630 $cm^{-1}$ appears, distinctive of unsaturated double bonds, which are products of saturated polymers under ozone attack. Under stress and ozone exposure the absorbance ratios increase indicating that the rate of ozone oxidation has increased.

Infrared spectroscopy has also been used to predict the service life of automotive coatings [9]. The coatings were "an acrylic melamine clear coat with a fully butylated melamine cross-linker" and, "an acrylic urethane clear coat with an isocyanate cross-linker". They were exposed to changing temperatures, irradiation levels and air pollutants. Evidence of new bands appearing in the spectra and intensity changes conformed to the mechanisms of degradation. Analysis of the results enables a prediction of degradation of the coatings to be made.

Perhaps one of the largest areas where spectroscopy has been used to study degradation processes is with regard to PVC. A paper by Bowley, Gerrard and Biggin indicates that plasticisers play an important role in the degradation [10]. The plastisicers added to PVC, such as dioctyl phthalate, dioctyl adipate and butyl benzyl phthalate. When the PVC is exposed to ultraviolet radiation, the formation of radicals occurs in the plasticisers. These radicals react with the PVC resulting in dehydrochlorination. Dehydrochlorination results in the formation of polyenes, which are observable using Raman spectroscopy. The effect of plasticiser radical formation resulting in degradation was then proven to be the case when an increase in the concentration of plasticisers resulted in an increase in the formation of polyenes. Therefore the degradation of PVC by weathering is observable by Raman spectroscopy.

PVC also degrades thermally. A study by Beltran and Marcilla demonstrates the use of *in-situ* infrared spectroscopy to study the degradation of PVC at temperatures in excess of 270 °C [11]. Changes in spectra below 140 °C have been related to

modifications in the crystalline and amorphous regions of the resin. At temperatures above 270 °C the formation of conjugated double bonds due to dehydrochlorination occurs. The appearance and disappearance of bands and band shifting is clearly observable in the spectra. It is in the 3100 → 3000 $cm^{-1}$ region that "stretching bands corresponding to C-H, =CH- and $=CH_2$ aliphatic of aromatic and non-aromatic rings, of conjugated double bonds, as well as the stretching bands of C-H from C=C=C-H", appear. The authors advocate that the polymeric chains are being transformed and double bonds are being formed showing that dehydrochlorination is occurring.

Raman spectroscopy also identifies the polyenes formed through dehydrochlorination, putting forward the evidence for the thermal degradation of PVC [12].

As can be surmised from the above examples, both infrared spectroscopy and Raman spectroscopy provide useful tools in the study of degradation for a variety of situations and processes. It is now time to turn to the study of the sealant PR14422 B2.

### 4.1.3 Degradation of sealant PR1422 B2

As briefly discussed in chapter 3 the aircraft sealant is exposed to a variety of factors, which may or may not lead to degradation. Therefore in order to understand the reason the sealant degrades it is imperative that all factors be considered and an understanding of any detrimental effects be gained. The sealant is constantly exposed to a mixture of aviation fuel and distilled water, temperatures ranging from –50 °C to +80°C and stresses as the wing moves when the aircraft is in motion. It has been shown in a paper by Carre et althat although a liquid may not exhibit any chemical reactivity towards a sealant the bulk properties of the adhesive may be altered [13]. The sealant may swell up resulting in an alteration of the viscoelastic properties. Other factors, which may be adversely affected, could be the reversible energy of adhesion and detachment. Paul *et al* show that dichromate cured polysulfides have superior resistance to swelling in hot water than those cured using manganese dioxide [14]. In the same paper it has also been shown that a high thiol content in aviation fuel can

lead to degradation in polysulfide sealants. This may occur through a thiol-disulfide interchange. Fuels containing a thiol content in excess of 0.04 % would act as sealant destroying fluids. Thermal degradation of the sealant alone is not thought to occur at operating temperatures as the paper mentions that a direct cleavage of the formal C-O or even the disulfide bond at temperatures as high as 180 °C is unlikely.

Thiol content in the fuel is not the only factor in fuel induced degradation of the polysulfide sealant. Stout discusses the appearance of sealant chalking after exposure to jet fuel [15]. The sealant in contact with the fuel deteriorates both physical and chemically. Analysis of the surface reveals that the sulphur content decreases and the presence of calcium carbonate increases as the chalk thickness increases. This results in calcium carbonate being the dominant material at the surface. Therefore the chalking is a concentration of the sealant fillers. Stout postulates that chalking occurs in the presence of metallic ions and mercaptans from the fuel. The fuel acts as an extractor either pulling fillers or polymers from the sealant. The presence of metallic ions (Fe, Ni, Cu, Cr, Zn and Si) has been detected in the chalking. They would have most likely come from fasteners and other hardware. Stout also relates the experience of sealant sponging where the sealant turns to a sponge rubber state. The critical variables are temperature and exposure to a fuel/$H_2O$ mix prior to exposure to higher temperatures. Stout concludes that a fuel/$H_2O$-saturated sealant has a much lower service temperature limit than previously thought.

The fact that the sealant is also exposed to water in the fuel tank should be taken into consideration. Water is one of the best solvents in chemistry and may have disastrous effects on polymers due to swelling phenomena, (see section 3.1.6).

There is no doubt that the presence of both aviation fuel and water has a detrimental affect on the sealant. This has been shown when sealant repair operations have been undertaken on aircraft that have been in-service for a number of years. The repair procedure demands that the integral sealant fuel tanks be completely dried out. The repair work is then carried out. However when the fuel tank is again filled with fuel more leaks appear that were not previously noticed. The reason suggested for this increased number of leaks is that the sealant has been swollen by the fuel/$H_2O$ and after drying out the sealant loses some of its volume.

Taking into account the operating conditions that PR1422 B2 experiences, the lower temperature of –50 °C is above the Tg for polysulfide polymers (Tg = -59 °C) and so this is not considered to have an adverse effect on the sealant. Also the sealant possesses rubber properties and so recovery from any stresses due to wing movement is believed to be complete. Therefore after discussion with British Aerospace representatives it was decided that the study should focus on fuel and water exposure at elevated temperatures.

Another factor to be considered is whether or not leaching of sealant material, be it the oligomers or fillers, is caused by exposure to aviation fuel or water.

### 4.1.4 Accelerated testing

As the deterioration of the sealant properties takes place over years rather than days an accelerated test had to be devised. This was done in order to simulate the effect of years of fuel and water exposure on a time scale measurable in a laboratory. The most common accelerated test for sealants is cyclic loading and environmental exposure where the material is exposed to the conditions it most commonly experiences but at their maximum level and at a much higher cycle rate.

A paper by Karpati states that load cycling of two-part polysulfide sealants is critical and leads to deformations and eventual disintegration [16]. Karpati subjected the cured sealants to varying extensions and compressions ranging from ±80 % to ±10 % of the joint width. Permanent deformation started to occur when the cyclic loading extended the sealant over 40 % of the joint width. Although Karpati shows that cyclic loading can lead to degradation of the sealant the conditions imposed are removed from those experienced by the sealant in fuel tanks.

Lacasse also simulates cyclic loading on two-part polysulfide sealants by using a mechanical vice [17]. The vice subjected the sealant to compression/extension cycles at an accelerated rate varying the cycle between ±10 % and ±80 % of the joint width. The results agreed with those of Karpati and again prove that accelerated cyclic loading is a very good approximation for the degradation that occurs for some

sealants. Lacasse also discusses cyclic exposure to environmental conditions and exposes the sealant to accelerated cycles of ultraviolet exposure and water exposure. Again the results show a correlation with environmental degradation of polysulfide sealants.

Stargel, investigating strain hardening in polysulfide sealants, also discusses cyclic loading experiments [18]. The cyclic loading of tension and compression which the sealant is subjected to result from temperature and humidity changes during day and night. Stargel bases his accelerated cyclic loading on the assumption that a sealant for the building trade last for a ten-year lifetime undergoing one cycle per day. Thus Stargel subjects the sealant to 3,000 cycles over an 8-hour period and a 24-hour period with a 25 % tension and a 25 % compression cycle. Stargel found no evidence for strain hardening.

Wernstähl uses accelerated exposure conditions to predict the service live of automotive coatings by correlating infrared measurements with the accelerated test [9].

Thus the use of accelerated testing is an accepted and standard method of testing the performance of sealants. For example the sealants used in buildings are repeatedly exposed to environmental elements both as the weather changes and the seasons change. Therefore an appropriate accelerated test which would take into account these varying conditions would be an accelerated cyclic load test using expansion and compression cycles and accelerated cyclic exposure to ultraviolet radiation and water.

It was decided that exposing the sealant to a Soxhlet extraction using aviation fuel and water at an elevated temperature would be the most suitable accelerated test for the examination of the degradation of the sealant PR1422 B2.

### 4.1.5 Peel-testing

The adhesive ability of a sealant is usually measured using the 180° peel test. This is the standard method of testing adhesion as used by the American Society of Testing Materials (ASTM). In the 180° peel test the sealant is subjected to a force which tears the sealant away from the substrate at an angle of 180°. The experiment is carried out at a constant peel velocity and constant temperature. The factors most commonly measured are the peel force and the method of failure. The failure mechanism is usually observed visually to determine whether cohesive or adhesive failure has occurred. The peel force, which is the force required to tear the sealant cohesively or adhesively, depends on the following factors: peel rate, peel thickness, temperature and the strength of the interphase.

Watts describes using the 180° peel test to help examine environmental degradation of polymer-to-metal adhesion [19]. In the paper, Watts exposes the sealant substrate samples to an accelerated environmental cycle, then peels the samples to examine whether adhesive or cohesive failure occurs.

In another paper by Karpati the 180° peel test is used to examine the failure mechanism and temperature dependence of adhesion [20]. Therefore the 180° peel provides a useful tool in sealant performance testing.

A paper by Shephard and Wightman exposes certain limitations in the peel test procedure [21]. They have shown that peel testing at one rate and thickness cannot adequately compare one sealant to another. They took a one-part acetoxy cured silicone sealant and embedded a fibreglass cloth in it before curing on a substrate. They peel tested the sample examining the adhesion to glass and aluminium substrates varying the peel velocity, the strained thickness and the sealant modulus.

Their results showed that the fracture energy for the higher modulus sealant (less unreacted polymer) is greater at low peel velocities than the fracture energy go the lower modulus sealant (more unreacted polymer). This suggests to Shephard and Wightman that the intrinsic fracture energy of the higher modulus sealant is greater than that of the low modulus sealant. However, their results show that the high peel

velocity data exhibits the opposite trend. Therefore the peel test shows differing results depending on the peel velocity.

For the case of the sealant PR1422 B2 as discussed in this chapter there was only the one sealant being examined and both the peel velocity and the thickness was constant for all samples.

## 4.2 Experimental

Separation methods : The most effective and convenient method of separation of additives in polymers is by extraction with a suitable solvent, using the Soxhlet apparatus and this is the technique used. The extraction process is extremely aggressive and in some cases may remove constituent oligomers from a polymer. The procedure involves the sample being continuously exposed to a liquid/vapour at high temperature (e.g. 60 °C). The liquid is constantly cycled thus aggressively attacking the sample if the sample is vulnerable.

### 4.2.1 Preparation of a new sealant mould

The sealant mould was constructed of poly (tetrafluoroethylene), {PTFE}, which because the sealant cannot wet it, prevents the sealant adhering to the mould. The sealant mould allowed the preparation of sealant specimens of dimensions 100 mm long, 25 mm wide, and ~4.5 mm thick. Figure 4.2.2 shows the components which made up the new sealant mould.

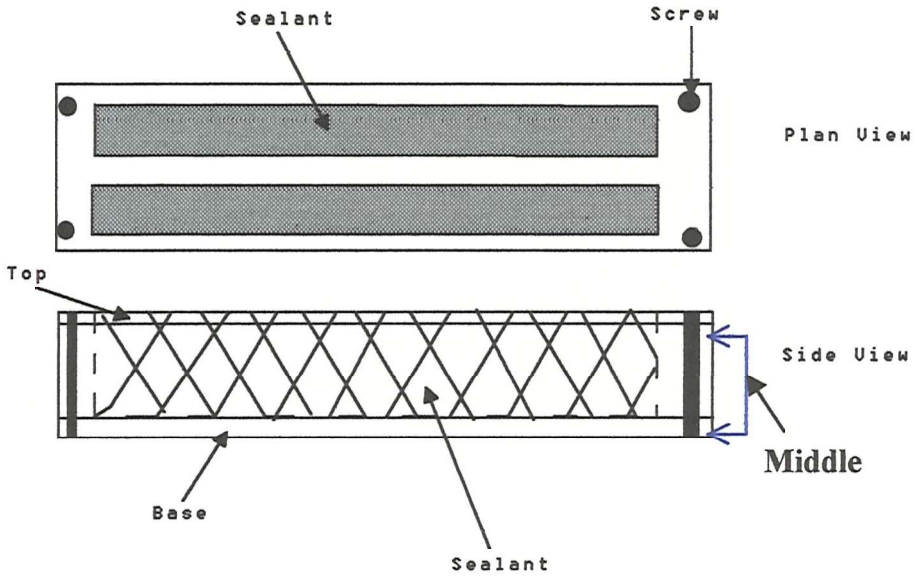


***Fig. 4.2.2*** *: Plan and side views of sealant mould. The sealant mould is made up of three parts, namely the top, middle and base sections. The top and middle sections have two cavities cut out into which the sealant is placed thus providing the mould for the specimens.*

### 4.2.2 Preparation of the peel test system

A peel test system was prepared. The system was used to peel test sealant specimens at 180° and determine the mode of failure. Figure 4.2.3 illustrates a sketch of the peel-test system. The sealant specimen is held in clamps, one at either end. One of the clamps moves relative to the other, at a controlled speed of 50 mm/min thus applying a peeling force on the sealant.

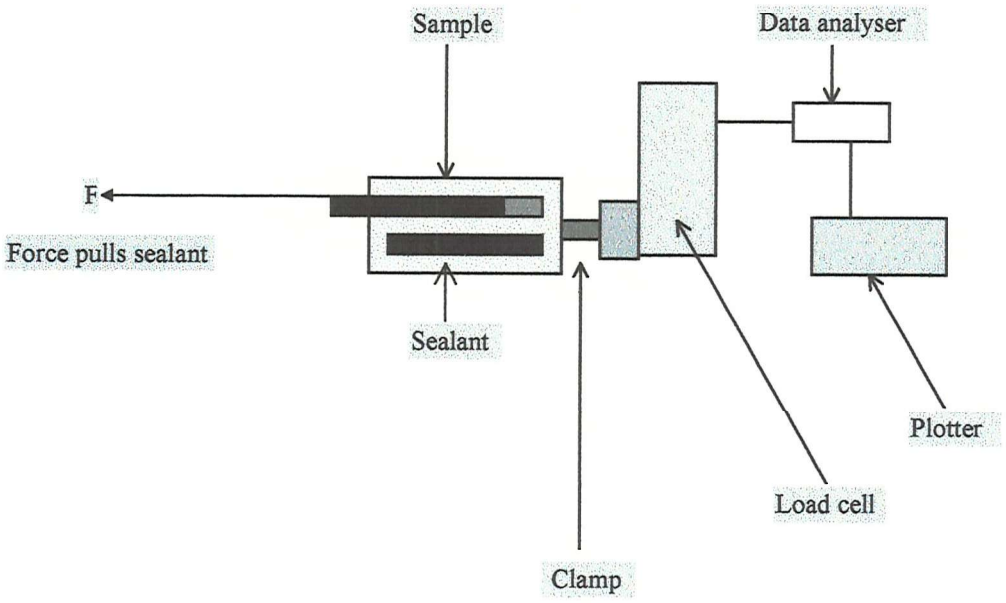


***Figure 4.2.3 :*** *The sample is peeled in a progressive manner revealing the mode of failure. The load cell records the force that is required to peel the sealant and the results can be plotted out if required.*

The load cell measures the force. As the force is applied the load cell experiences the force reaching a maximum just before the sealant tears or peels. When the sealant begins to peel the load cell records this force thus giving an indication of the relative strengths of the bonds for different adhesives and differing conditions.

The data analyser converts the forces experienced by the load cell into readable data and this data can then be recorded. The data is usually recorded on a plotter which, shows the forces applied on the sealant over time. Analysis of the plot will reveal the force required to peel the sample.

In order to begin the peel on a sample, a clean cut through the sealant and perpendicular to the applied force was executed with a razor blade. These cuts were repeated at regular intervals, for example every 3-cm, so that data on a number of peels can be obtained from the one sample. Examination of the torn sealant specimen revealed whether adhesive or cohesive failure occurred.

### 4.2.3 Preparation of ideal seals

After instruction by a BAe representative, test ideal seals were prepared using materials supplied by BAe as discussed in chapter 3. These were PR1422B2 sealant on PR143 primer paint, which was abraded and cleaned. Using the sealant mould the sealant specimens were prepared by applying the sealant to the middle section into the two cavities. When the cavities were full, wire gauze was placed over the sealant. The wire gauze is gripped by a clamp in the peel test system and is pulled back at 180° to peel test the sample. The top section was placed on the mould and the sealant was applied into the cavities so that the wire gauze was embedded in the sealant. They were left for 14 days at room temperature and humidity in order to cure before experimental work was carried out.

### 4.2.4 New accelerated test procedure for secondary seal performance

It was decided that the Soxhlet extraction method was the most suitable accelerated test. A temperature of 60 °C was decided upon and the fuel used was a synthetic fuel consisting of 2,2,4-trimethyl pentane (30% v/v) and toluene (70% v/v). Sealant specimens using sealant PR1422B2 base mixed with the appropriate accelerator in a ratio of 10:1, base:accelerator by weight were placed in the sealant mould and left to partially cure for 24 hours. It was also decided to trial the sealants PR1779 and PR1221B2 in the Soxhlet as these were known to pose particularly bad deterioration problems. The samples were then removed from the mould and left to finish curing in a fume cupboard over a period of 14 days. The sealant specimens were then taken and placed in the Soxhlet extraction system using the synthetic fuel previously described, as the extracting solvent at a temperature of 60 °C for a period of 1 month.

### 4.2.5 Examination of sealant specimens after the accelerated test.

The sealants and solvents were examined visually before the sealant specimens were subjected to the load-test. ATR-IR and Raman spectra of any material extracted into the solvents were attempted.

## 4.3 Results and Discussion

### 4.3.1 Analysis of sealant samples after acceleration test.

Initially tests using the solvent system already mentioned (section 4.2.4) failed. The sealant remained unaffected by the solvent. In other words the solvent was not aggressive enough and did not correspond closely enough with the fuel mixture experienced by the sealant during its lifetime. On discussion with BAe it was decided to change the solvent to one more indicative of the aviation fuel used in aeroplanes. This solvent consisted of 59% v/v toluene, 30% v/v cyclohexane, 10% v/v 2,2,4 trimethyl pentane and 1% v/v dibutyldisulfide. With this new solvent in the Soxhlet extraction system, physical and chemical changes of the various sealants were examined.

### 4.3.2 Visual test

Sealant PR1422B2 looked unaffected by the accelerated test. The solvent was a pale green colour indicating that some constituents of the sealant had been removed.
Sealant PR1779 also looked unaffected by the accelerated test. The solvent was a yellowish colour again indicating that the Soxhlet extraction had indeed removed constituents from the sealant.
Sealant PR1221B2 was totally destroyed by the accelerated test. The sealant had broken up. The solvent was a brown colour and produced a stench similar to sulphur.

### 4.3.3 Mass differences

Sealant PR1422B2 had an initial mass of 47.2228 g before the accelerated test. After the accelerated test the mass had fallen to 46.4692 g. The sealant was left in an oven, at 40 °C, until a reproducible mass was obtained. This mass was 45.4068 g indicating an overall loss of 1.7160 g, or 3.6 %.
Sealant PR1779 had an initial mass of 44.6740 g before the accelerated test. After the accelerated test the mass had risen to 45.3153 g. The sealant was left in an oven until a reproducible mass was obtained. This mass was 43.6590 g indicating an overall loss of 1.0150 g, which is a loss of 2.4 %.

Sealant PR1221B2 had an initial mass of 50.9236 g before the accelerated test. After the accelerated test the mass had fallen to 37.4856 g which is a loss of 24.4 %.

| Sealant | Initial Mass (g) | Final Mass (g) | Mass Difference (g) | Mass Difference (%) |
|---|---|---|---|---|
| PR1422 B2 | 47.2228 | 45.4064 | 1.7164 | 4 |
| PR1779 | 44.6743 | 43.6591 | 1.0152 | 2 |
| PR1221 B2 | 50.9236 | 37.4856 | 13.438 | 26 |

***Table 4.3.1:*** *The mass differences for the sealants after Soxhlet extraction.*

### 4.3.4 Load test

Sealant PR1422 B2 passed the load test producing a cohesive failure. Force required was 139 N, (minimum requirement of 90 N).
Sealant PR1779 passed the load test producing a cohesive failure. Force required was 114 N.

### 4.3.5 Presence of Chalking

The samples did show some evidence of chalking. The white chalk-like material was carefully removed and examined. It proved to be calcium carbonate and assigned to one of the fillers. The filler therefore is pulled out of the sealant body by the fuel. This reduces the volume of the sealant and it is probable that fuel or water may migrate into the voids and interact with the interior of the sealant. New sealant formulations will have to take account of this extraction of filler and preferably prevent this occurring.

### 4.3.6 Infra-red spectra of the solvents and sealant specimens

ATR spectra were recorded of the material extracted by the solvent. These spectra may be viewed in Figures 4.3.1-4.3.5. Those figures (4.3.4-5) of the material extracted from sealant PR1422 B2 show the presence of many similar vibrations to

the vibrations featured in the sealant spectra. This would suggest that it is actually polymer oligomers, which are being extracted.

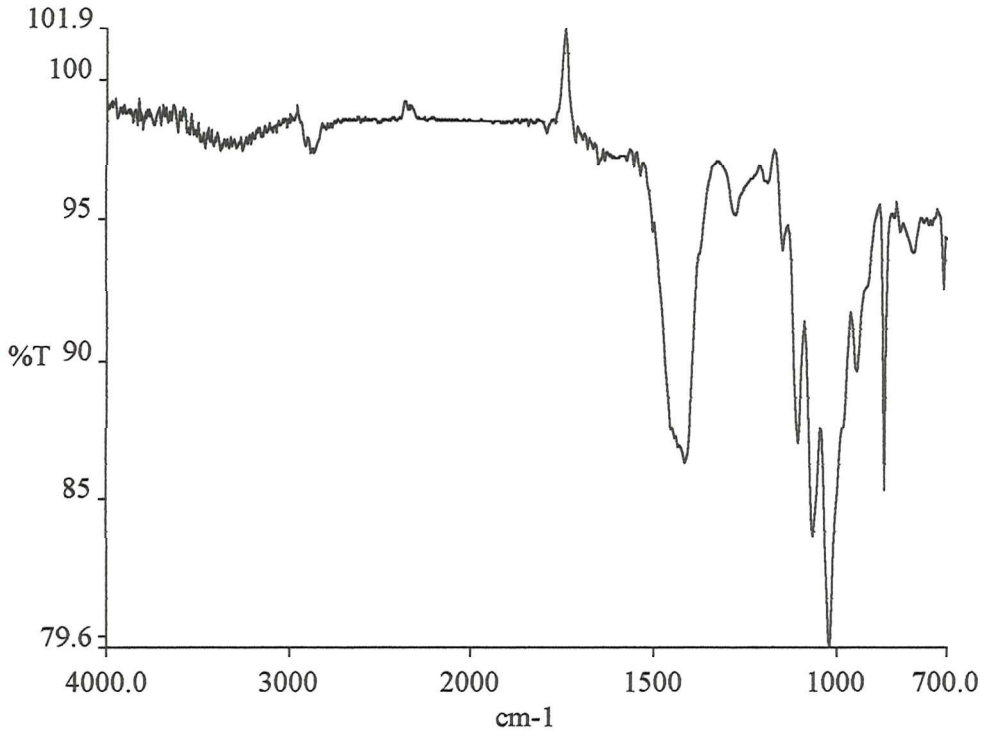


***Figure 4.3.1 :*** *ATR spectrum of sealant before being exposed to a Soxhlet extraction.*

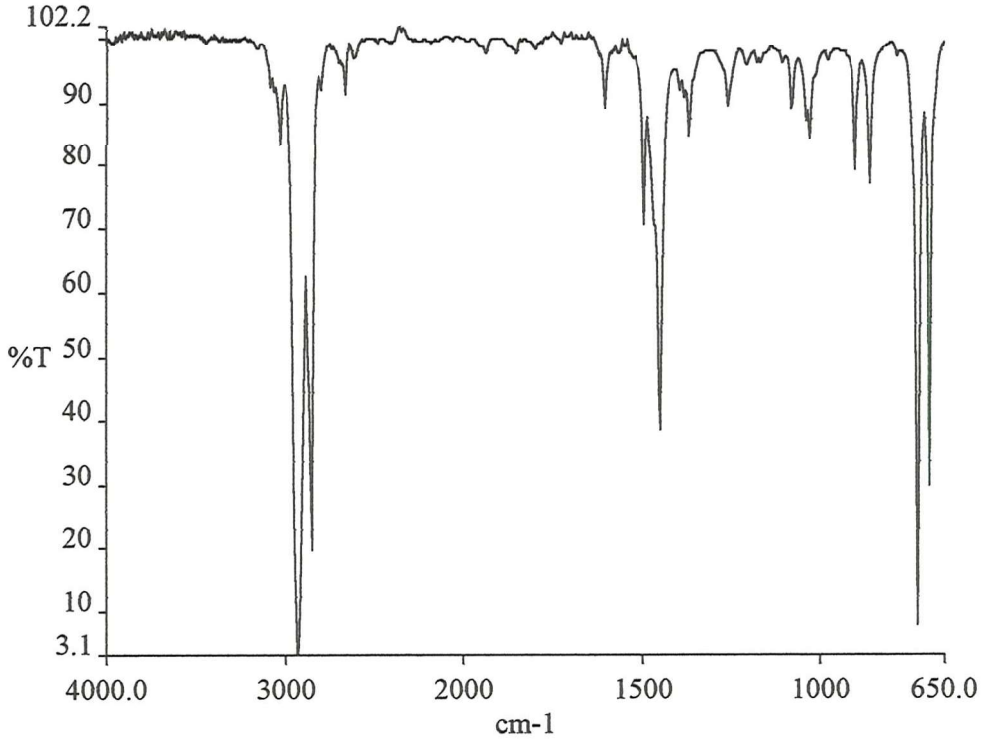


***Figure 4.3.2 :*** *ATR spectrum of the synthetic fuel used in Soxhlet extraction*

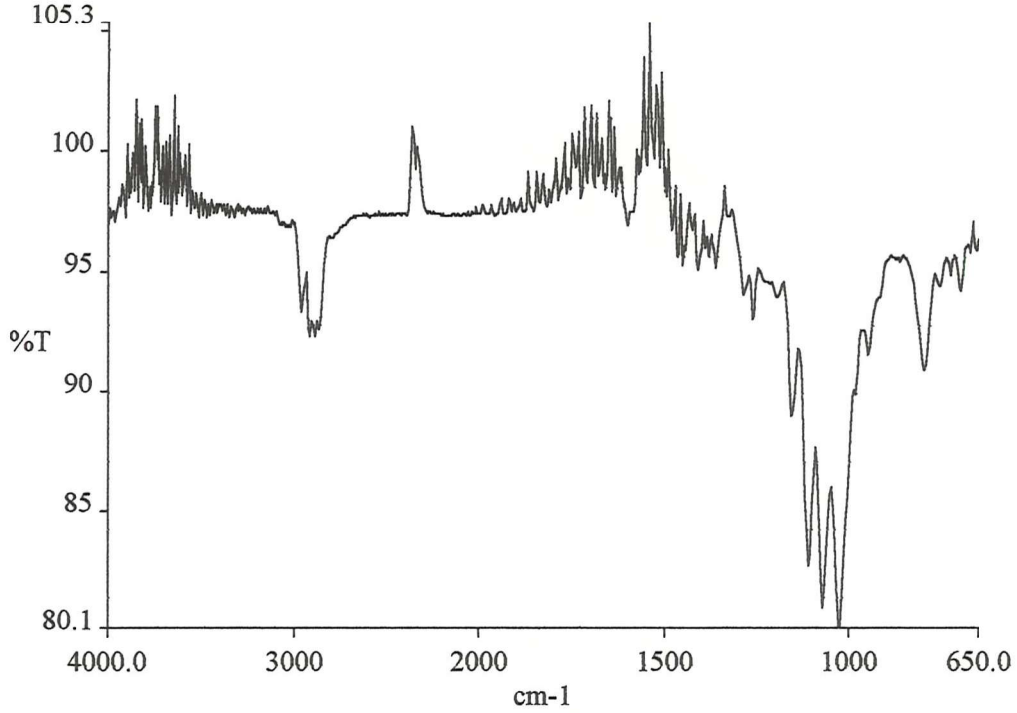


***Figure 4.3.3 :*** *ATR spectrum of sealant after Soxhlet extraction.*

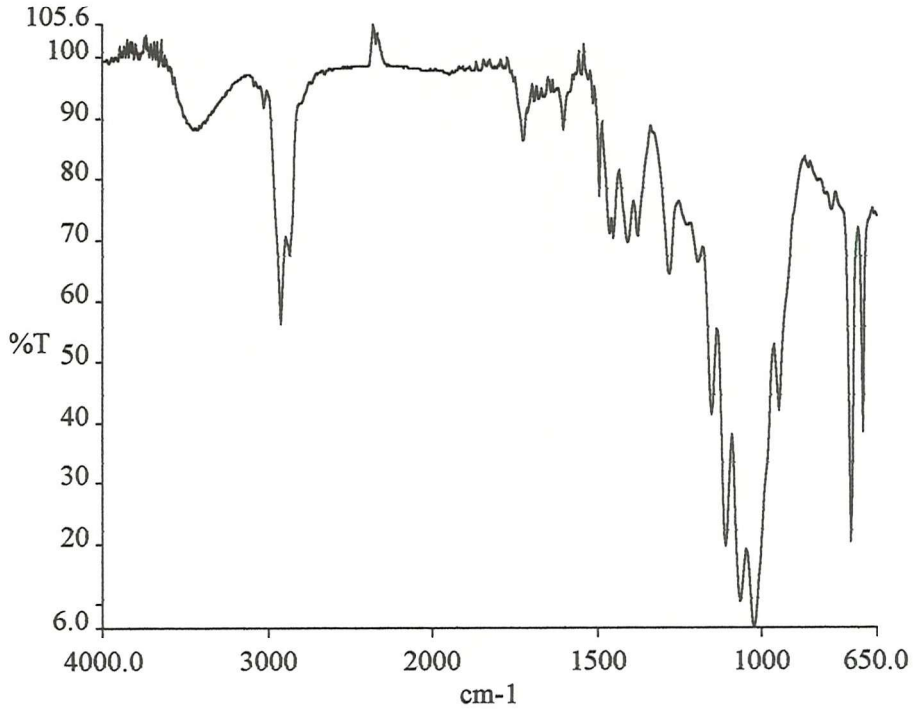


***Figure 4.3.4 :*** *ATR spectrum of material extracted from sealant*

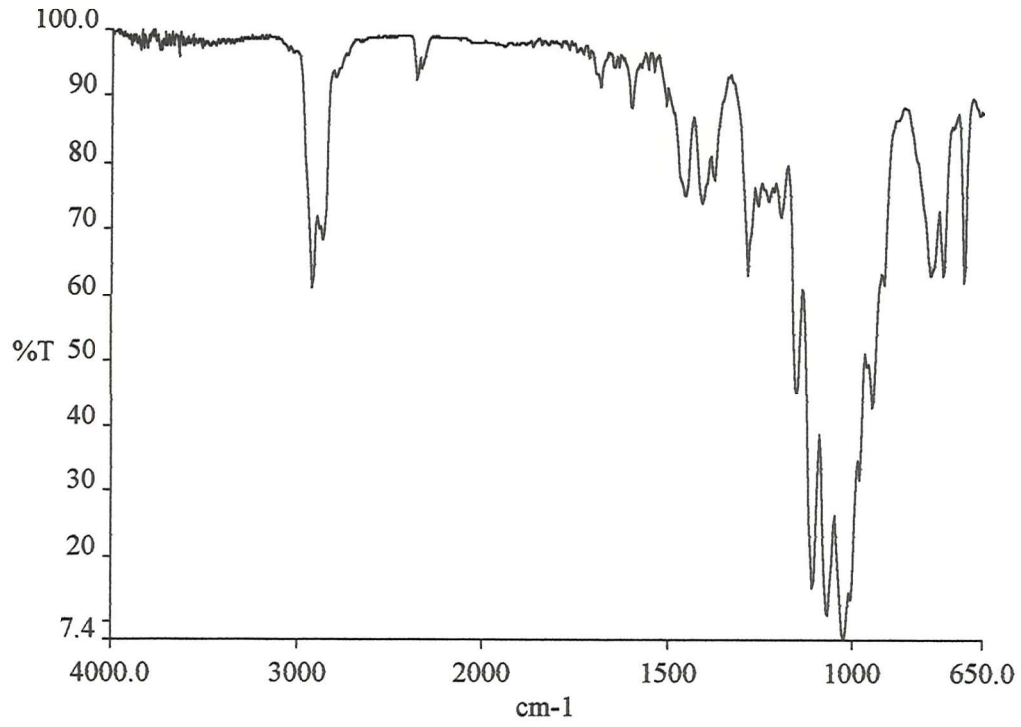


***Figure 4.3.5*** *: ATR spectrum of material extracted from sealant after rotavacuuming.*

There are differences to be noted between the Figure 4.3.1 and Figures 4.3.3-5. The most visible changes are the complete disappearance of the peak at 873 $cm^{-1}$ and the large reduction of the broad band at ~1417 $cm^{-1}$. The peak at 873 $cm^{-1}$ has been previously assigned to either a C-O-C symmetric stretch, a C-H bend or epoxide in Chapter 3. There is also a reduction in the peak at 1069 $cm^{-1}$ which has been also assigned to the –C-O-C- symmetric stretch in Chapter 3. The appearance of new bands at 732 $cm^{-1}$ and 696 $cm^{-1}$ in Figure 4.3.4 is due to fuel residue contaminating the sample (cf. Figure 4.3.2). In Figure 4.3.5 these peaks are reduced after rotavacuuming. There is also a new peak at 799 $cm^{-1}$ which has not been possible to positively identify. It may be due to –C-H bend.

The spectra clearly show that there appears to be polymeric material extracted from the sealant by the fuel. This will have disastrous affects on the performance of the sealant as the volume is being reduced, leak pathways are being introduced and fuel and water can penetrate the interior of the sealant. Leaching of material from the sealant thus must result is a deterioration of the performance of the seal. Failure of the sealant is an inevitable result over time.

### 4.3.7 Raman spectra of sealant

Raman examination has so far proved unsuccessful with both material extracted into the solvents and with the sealant specimens. The sealant specimens burned under the power of the laser. It is hoped in the future that by rotating the sealant specimens in the laser beam a Raman spectrum will be recorded. No spectrum was produced from the rotavacuumed down samples of extracted material.

### 4.3.8 Separation of the constituents in the material extracted

TLC plates were prepared with samples from each of the Soxhlet extractions. It was found that the materials extracted were very complex mixtures and were impossible to separate completely. It was decided that any further chromatographic method of separation would be worthless.

## 4.4 Conclusion

This chapter has shown the benefits of using an accelerated cyclic test followed by a 180° peel test in order to test the durability of sealants used in integral fuel tanks of aircraft. Both of the sealants PR1779 and PR1221 B2, known to pose deterioration problems, underwent deterioration in the examination. Also the sealant PR1422 B2 also demonstrated deterioration and thus as this is the sealant most commonly in use a careful rethink of the formulation of this sealant is urgently required. The loss of sealant filler is a concern and will have to be examined.

Deterioration of the sealant samples was clearly evident from infrared spectroscopy. Infrared spectroscopy was used to help identify the deterioration products and thus identify the method by which deterioration occurs. The results show that it is the polymer oligomers that are being extracted by the fuel. New sealants will therefore have to be resistant to this extraction process. Accelerating testing should also be carried out using water and a combination of fuel and water as the solvents in Soxhlet extractions.

Correlating the sealant exposure to the Soxhlet extraction, to actual service time is required so a prediction of the lifetime of sealants would be possible. This chapter does not propose any method to improve sealants and further work should be carried out in this field.

**References:**


1. N.J. DiNardo, *Proc. Int. Conf. Vac. Web. Coat.*, **5**, (1991).
2. N.A. Thorne, P. Thuery, A. Frichet, P. Gimenez, A. Satre, *Surface and Interface Analysis*, **16**, 1-12, (1990).
3. C.A. Wilkie, M.L. Mittleman, in *Themogravimetric Anaylsis – IR Spectroscopy, Chpt. 9; J. Appl. Polym. Sci.*, **42**, 901, (1991).
4. B.A. Horn, J. Qui, N.L. Owen, W.C. Feist, *Applied Spectroscopy*, **48**, 6, (1994).
5. S. Higuchi, T. Hamada, Y. Gohshi, *Applied Spectroscopy*, **51**, 8, (1997).
6. E. Schoenberg, H.A. Marsh, S.J. Walters, W.M. Saltman, *Rubber Chemistry and Technology*, **52**, 582, (1979).
7. R.W. Layer, R.P. Lattimer, *Rubber Chemistry and Technology*, **63**, 427, (1990).
8. S.G. Hong, C-M. Liao, *Polymer Degradation and Stability*, **49**, 3, (1995).
9. K.M. Wernstähl, *Polymer Degradation and Stability*, **54**, 1, (1996).
10. H.J. Bowley, D.L. Gerrard, I.S. Biggin, *Polymer Degradation and Stability*, **20**, 2, (1988).
11. M. Beltrán, A. Marcilla, *Eur. Polym. J.*, **33**, 7, (1997).
12. K.P.J. Williams, D.L. Gerrard, Eur. Polym. J., 26, 12, (1990).
13. A. Carre, J. Schultz, *J. Adhesion*, **18**, 3, (1984).
14. D.B. Paul, P.J. Hanhela, R.H.E. Huang, *Polym. Sci. Technology*, **37**, 269, (1988).
15. R.J. Stout, *Natl. SAMPE. Tech. Conf.*, **13**, 64, (1981).
16. K.K. Karpati, *Durability of Building Materials*, **5**, 1, (1987).
17. M.A. Lacasse, *ASTM Spec. Tech. Stp. 1254, (Science and Technology of Building Seals, Sealants, Glazing and Waterproofing)*, **3** ,5, (1994).
18. S. Stargel, *J. Elastoplastics*, **3**, Oct., (1971).
19. J.F. Watts, *Surface and Interface Analysis*, **12**, 1-12, (1988).
20. K.K. Karpati, *J. Paint Technology*, **45**, 580, (1973).
21. N.E. Shephard, J.P. Wightman, *ASTM Spec. Tech. Publ. Stp. 1271, (Science and Technology of Building Seals, Sealants, Glazing and Waterproofing)*, **5**, 226, (1996).

# Chapter 5

# A Raman study of the polymers polypropylene and polyethylene terephthalate at high temperatures

# Chapter 5

# A Raman study of the polymers polypropylene and poly(ethylene terephthalate) at high temperatures

## 5.1 Introduction

This chapter focuses on the Raman study of polypropylene and poly(ethylene terephthalate) at temperatures just below, at and just above their melting points. It investigates whether order, in the form of regularity bands, present in the polymers below their melting points is retained at temperatures above their melting points.

### 5.1.1 Vibrational spectroscopy study of polypropylene

Polypropylene is found in three isomeric forms, isotactic, syndiotactic and atactic. The isotactic form is by far the most commercially important and has been studied the most extensively by vibrational spectroscopy. In isotactic polypropylene (iPP) the individual chains in the crystalline order lie in $3_1$ helices, with each unit cell containing four chains [1,2]. Two of these screw upwards and two down to produce a space group $C_{2h}$. Normal co-ordinate analysis has been performed on the assumption that the vibrational characteristics are those of a single chain [3-5]. These chains would only have a $C_3$ symmetry. Polarised infrared studies have been extensively carried out.

Raman spectra have been recorded with increasing success by Tobin, Malakov and Schaufele [6-8]. Polarisation studies have been carried out on monoclinic, smectic and the melt of isotactic polypropylene using conventional Raman spectroscopy [9]. FT-Raman spectra and an assignment of the bands can be found in reference [10]. Usually, the analyses are based upon the line group but an attempt has been made to assign the Raman spectra on the basis of the space group [2]. Several attempts have also been made with varying degrees of sophistication to record anisotropic scattering on oriented polypropylene [11]. The mid-infrared spectrum of isotactic polypropylene has been assigned with good agreement between the various authors [12-14]. The mid-

infrared spectrum has been shown to be free of crystallinity bands, i.e. vibrations due to an ordered 3-dimensional structure. Studies have also been carried out on the far-infrared spectrum of isotactic polypropylene where spectral features have been attributed to intermolecular vibrations [15-17]. Information has also been obtained using inelastic neutron scattering [18,19].

### 5.1.2 Regularity bands in polypropylene

An important feature of the vibrational spectrum of iPP is regularity bands. These are dependent upon the conformation of individual chains that arise from sections of the chain, which have the $3_1$ helical structure. These features should disappear upon melting the polymer as the helices are destroyed. On this basis it has been established that regularity bands occur at 809, 841, 900, 973, 998 and 1220 $cm^{-1}$. It should be noted that the band at 973 $cm^{-1}$ also has a component from chains in disordered regions, which have irregular conformations.

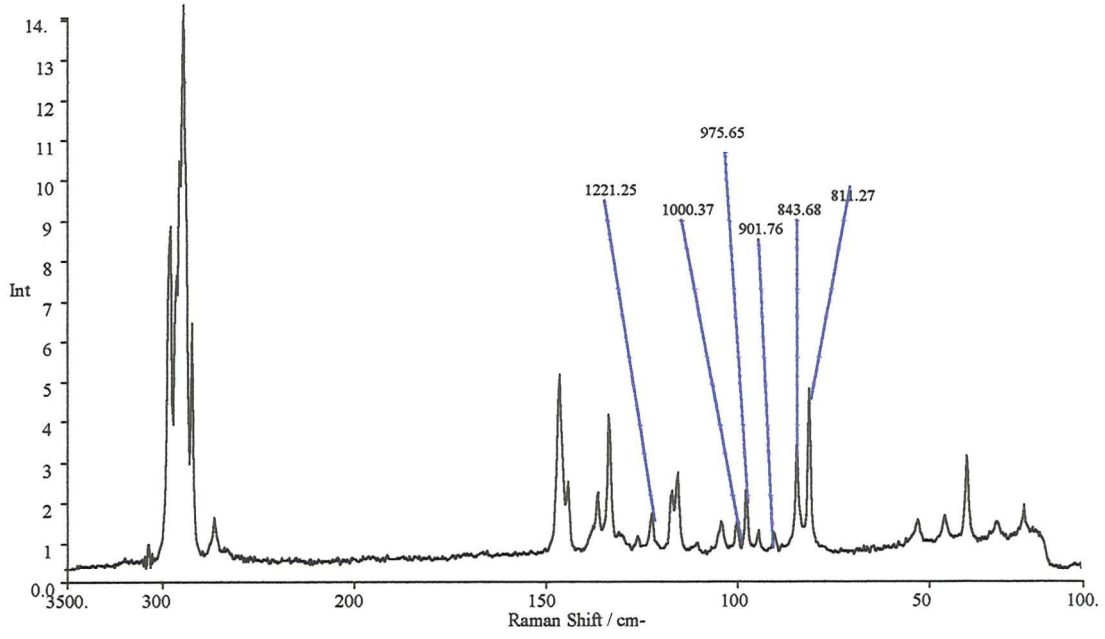


**Figure 5.1:** *FT-Raman spectrum of isotactic polypropylene with regularity bands labelled.*

### 5.1.3 Regularity bands and sequence lengths

Several authors have shown that these regularity bands only appear for minimum helical sequence lengths. Methods used include studies on copolymers of iPP, thermal degradation and changes in band intensity studies upon stretching (V. Zichy, unpublished report) all using infrared techniques [20-22]. The minimum sequence length for the 998 $cm^{-1}$ band is between five and ten propylene units. The band at 843 $cm^{-1}$ has a minimum sequence length of ≈ 13 while the others are associated with longer sequences of at least 15. This was taken advantage of by Hendra *et al* who used change in the intensity of the regularity bands to gain structural information on iPP at temperatures below its melting point [23].

| Raman frequency, $cm^{-1}$ | Raman intensity | Infra-red frequency, $cm^{-1}$ | Infra-red intensity | Symmetry | Assignment |
|---|---|---|---|---|---|
| 1220 | s | 1218 | vw | E | $tCH_2+\delta CH+\nu C-C$ |
| 998 | m | 998 | m | A | $rCH_3+\omega CH_2+\delta CH$ |
| 973 | s | 974 | m | A, E | $rCH_3+\nu C-C$ chain |
| 900 | m | 900 | w | A, E | $\nu CH_3+rCH_2+\delta CH$ |
| 841 | vs | 841 | m | A | $rCH_2+\nu C-CH_3$ |
| 809 | vs | 808 | w | A, E | $\nu CH_2+\nu C-C$ + $\nu C-CH$ |

**Table 5.1:** *Details of the regularity bands of iPP.*

As Zerbi noted, the band at 988 $cm^{-1}$ is still visible in the infrared spectrum 5-10 °C above the melting point implying some short range order (of at lest five units) persists in the melt [24]. Making conventional Raman measurements Vasco and Koenig extended this report [9]. The aim of the work in this chapter is to further extend this work by repeating the experiment with accurate variable temperature control in an attempt to establish the temperature at which short range order in the melt is lost.

### 5.1.4 Vibrational spectroscopy study of PET

The experiment is repeated for PET in order to establish if there is any short-range order in the melt as speculated by Hendra [25]. PET exists in two phases, the crystalline and amorphous although there are claims that a third partially ordered phase exists (see below). The crystalline phase contains a bond that are *trans* around the ethylene glycol linkage whilst the amorphous region contains both *gauche* and *trans* rotamers [26]. There is a linear relationship between the trans isomer content and the degree of crystallinity [27]. Miyake has shown that some bands in the infrared spectrum increase in intensity with some crystallinity while others decrease [28]. McGraw has shown that four Raman bands increase in intensity with crystallinity, 1096, 1000, 857 and 278 $cm^{-1}$ [29]. The FT-Raman spectrum of PET is shown in Figure 5.2, with assignments given in Table 5.2.

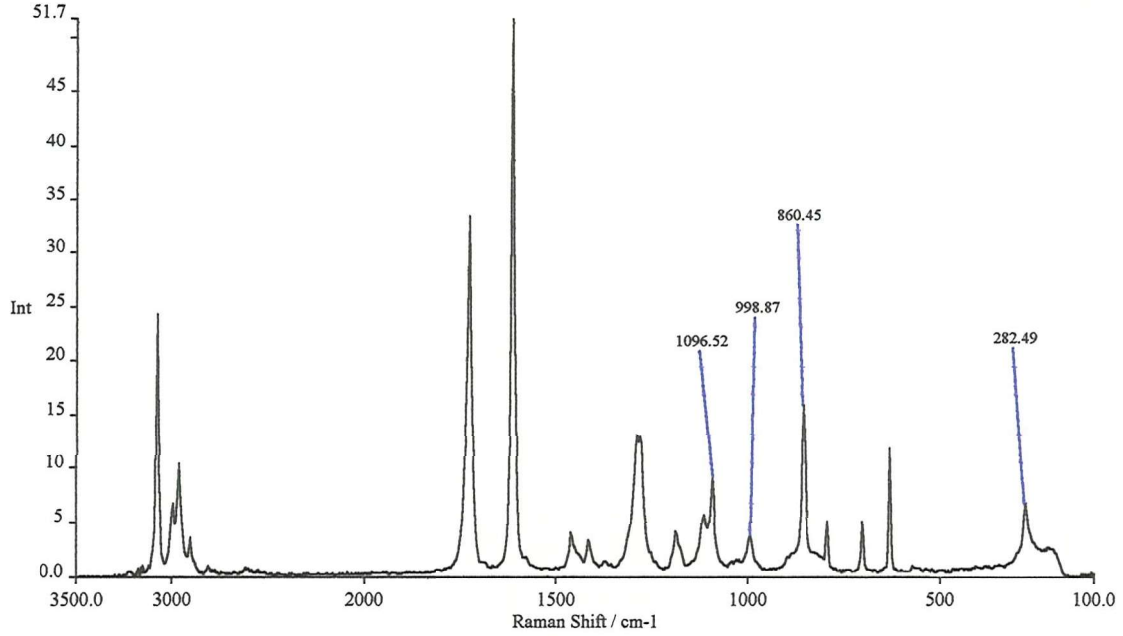


**Figure 5.2:** *The FT-Raman spectrum of PET with regularity bands labelled.*

| Raman frequency, $cm^{-1}$ | Raman intensity | Assignment |
|---|---|---|
| 1096 | s | νO-CH2 |
| 1000 | m | νC-C |
| 857 | s | νC-X |
| 278 | m | δCX or δring |

**Table 5.2:** *Details of the regularity bands in PET.*

There are possibly three phases of PET, a situation demonstrated by Wunderlich using X-Ray diffraction and confirmed by Ruvolo-Filho and de Carvalho using solvent absorption techniques [30,31]. Along with amorphous (disordered) and crystalline (3-dimensionally ordered) there is also a mesomorphic phase consisting of a 2-dimensionally ordered structure.

This work shows the presence of 2-dimensionally ordered material in the melt for a few degrees above the melting point. This shows that trans isomers can arrange into some sort of short-range order in a disordered environment. This strengthens the case for a third phase in the solid.

### 5.1.5 High temperature Raman spectroscopy

High temperature Raman spectroscopy has been carried out by many groups [32-34]. This is normally attempted using a conventional Raman spectrometer and a laser emitting in the visible. Hot samples are black body radiators the intensity of which increase with temperature. If a visible laser is used, the black body emission effectively falls outside the Stokes Raman domain. When transferring this experiment to FT-Raman spectroscopy using a laser operating at 1.064 μm the Stokes range now extends from 1.064 μm to 1.7 μm and at temperatures in excess 150 °C black body radiators interfere with the Raman spectrum. As the temperature rises an ever-stronger background appears increasing towards large shifts until eventually its intensity is such that the detector/preamplifier saturates and no further increase in temperature is worthwhile. The noise in a FT spectrum whether it be infrared or Raman is related to the integrated intensity of the collected light. Hence, high backgrounds produce noisy spectra. Spectra are routinely recorded up to approximately 180 °C using FT-Raman but above this the black body emission is normally too intense [35].

Several ingenious ways of reducing or eliminating the black body emission have been demonstrated. Bennett used a laser where the output varied sinusoidally at ≈ 500 Hz and used wave mixing and subsequent Fourier analysis to discriminate between the Raman and the black body radiations [36]. Earlier, Cutler used a laser varying in intensity at a much higher frequency and used phase sensitive detection to

discriminate the Raman signal from the total emission [37]. Both approaches are clever but complex and hence expensive to employ.

The aim of this work was to record FT-Raman spectra of polymers through their melting points, i.e. at temperatures up to and well above 200 °C. The cell used in this work was not only capable of reaching elevated temperatures but was also able to control them to within ±0.5 °C. This results in our ability to monitor changes in the selected polymers spectra (and hence their structure) as they approach, pass through and go beyond their melting point.

## 5.2 Experimental

All spectra were recorded on a Perkin Elmer system 2000 Raman spectrometer as discussed in chapter 2.

A specially designed cell as produced by Ventacon Ltd.; (Model H) was used to reach the high temperatures (up to 300 °C). A type J thermocouple and a modified Model D1 Ventacon Universal temperature controller and power supply allowed temperature monitoring and control. Thus it was possible to maintain temperatures to better than ±0.5 °C of the set temperatures. In order to attenuate the radiation to the red of 1490 nm a filter was fitted into the filter wheel of the spectrometer. This prevented all the radiation beyond 2400 $cm^{-1}$ reaching the detector. Although this results in the loss of some spectral information this was not a drawback. Thus, it was possible to record FT-Raman spectra for temperatures well in excess of 200 °C. The action of the filter can be seen in Figure 5.3. Although there is a minimal drop in intensity across the entire spectrum there was no adverse affect on the results.

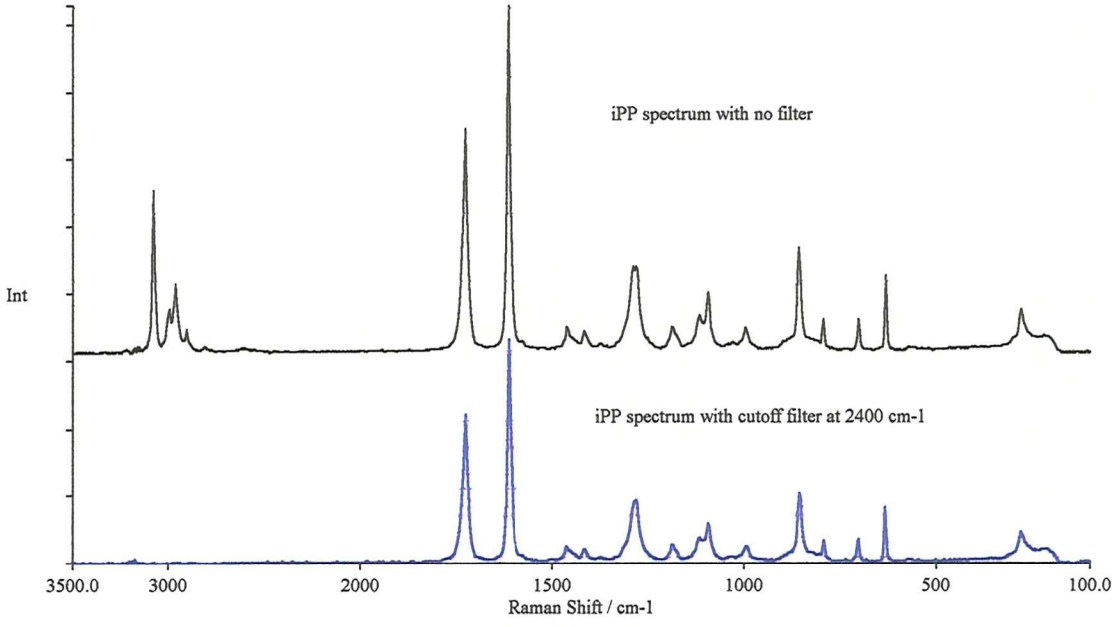


**Figure 5.3:** *The FT-Raman spectrum of iPP with and without a cut-off filter at 1490 nm. Both spectra recorded under otherwise identical conditions.*

The iPP sample used possessed a melting point near 189 °C and therefore spectra were recorded at 160, 170, 180, 185, 190, 195, 200 and 210 °C. The PET sample used had a melting point around 260 °C and therefore spectra for this sample were recorded

at 200, 240, 250, 260 and 265 °C. The detector became overloaded with black body radiation at higher temperatures.

## 5.3 Results and Discussion

### 5.3.1 Results for polypropylene

The spectrum of iPP recorded at different temperatures is shown in Figures 5.4 and 5.5.

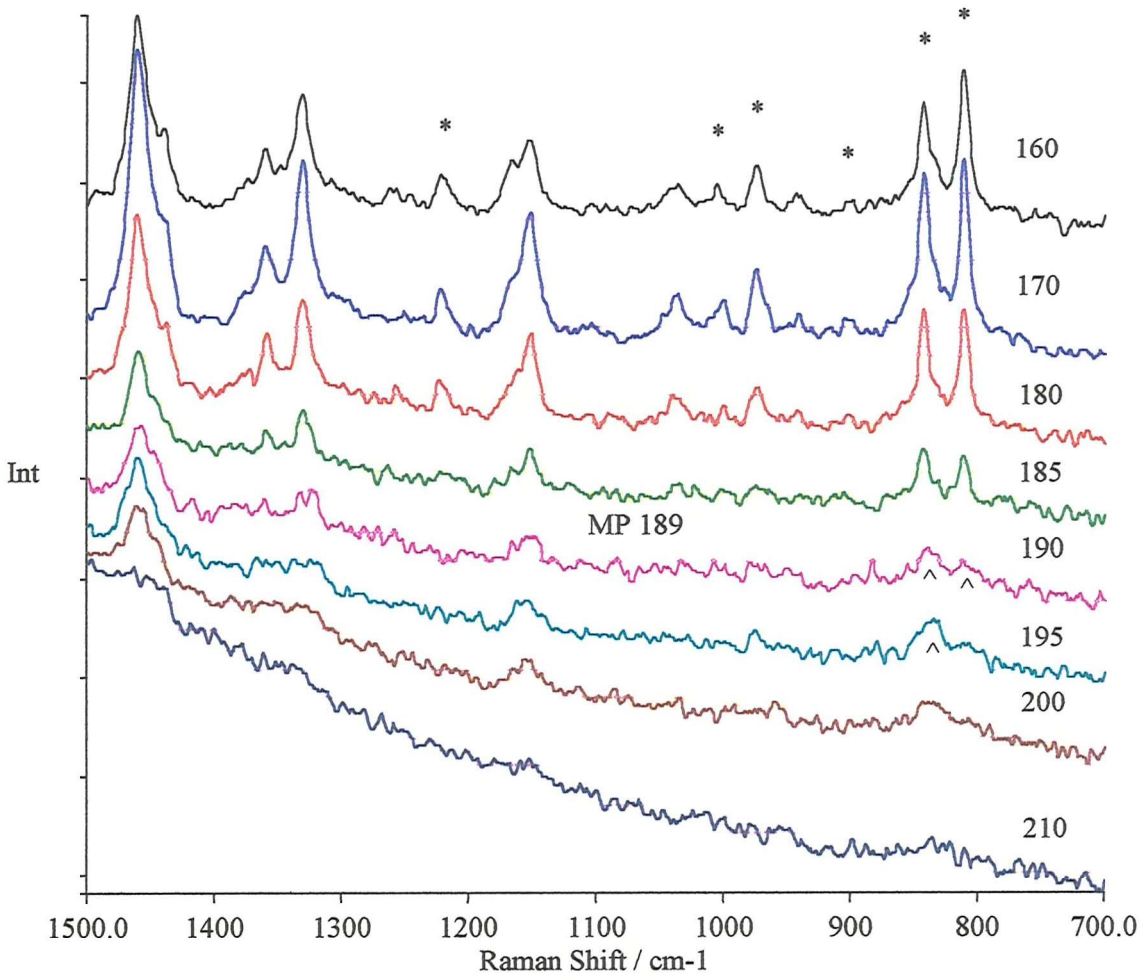


**Figure 5.4:** *The Raman spectra of iPP at various temperatures. The regularity bands are labelled *. All temperatures are in °C. Regularity bands visible above the melting point are labelled ^.*

Clearly visible in these spectra are peak broadening and peak shifting as the temperature is increased. The peak shifting may be due to expansion of the unit cell upon heating. This affects the environment of the vibrating groups and therefore the frequency. As the temperature is increased the number of defects in the crystalline region increases causing rapid changes near the melting point. This causes the peak to broaden. The peak shift for the band at 1461 $cm^{-1}$ is clearly visible in Figure 5.5. A

plot of wavenumber versus temperature for the band at 1461cm$^{-1}$ can be seen in Figure 5.6.

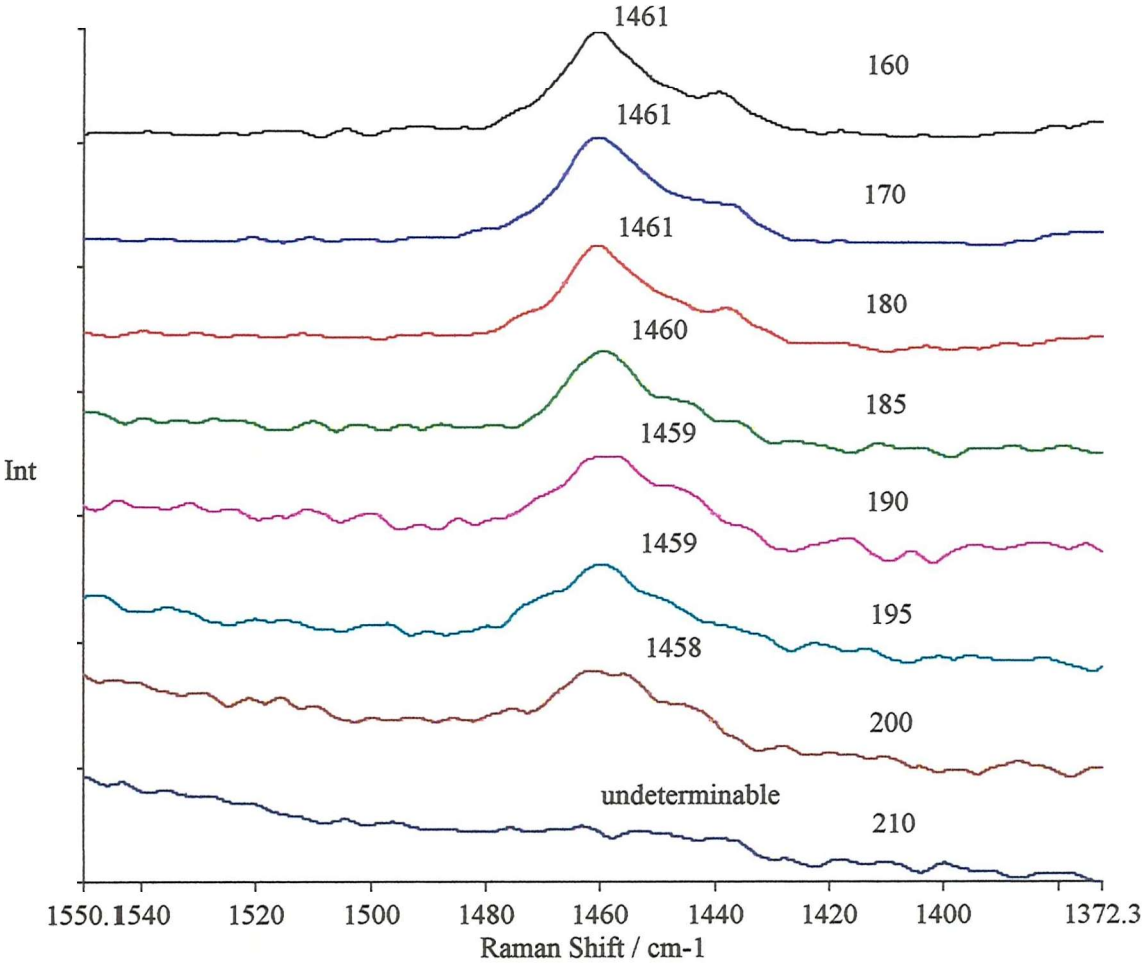


**Figure 5.5:** *The FT-Raman spectra of the band at 1461 cm$^{-1}$ at various temperatures. A shift is clearly visible.*

As discussed in the introduction (section 5.1.2) there are six Raman bands which could indicate the short-range order in the melt of iPP. They are at 1220, 998, 973, 900, 841, 809 cm$^{-1}$. It should be noted at this point that Raman intensity particularly in FT spectrometers is very sensitive to turbidity. As the polymer is melted it becomes clear, the scattering volume decreases and the intensity drops even after allowing for the broadening of the bands. The effects visible above the melting point are therefore all the more obvious. Possibly the most significant feature in Figure 5.4 are the changes in the spectra as they pass through the melting point. At 185 °C regularity

bands are definitely visible but as the temperature reaches 190 °C they have almost disappeared.

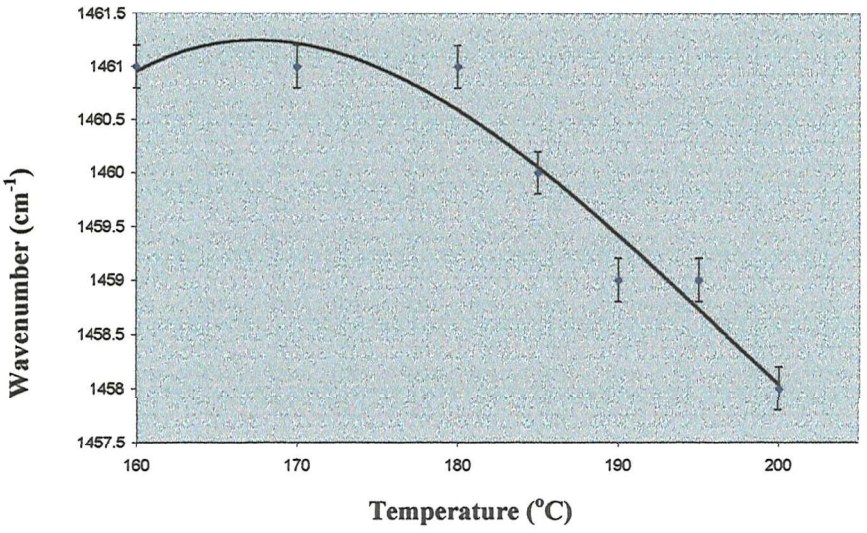


**Figure 5.6:** *Plot of temperature versus wavenumber of the band at ≈1461cm$^{-1}$ for iPP. The melting point is at 189 °C.*

As the temperature increases (near the melting point) and the bands broaden several of the regularity bands disappear. These peaks are already weak in the spectra taken at 160 °C and vanish rapidly upon heating. It has been established using infrared spectroscopy that the band at 1000 cm$^{-1}$ is due to short-range order of approximately 5-10 units long. It was hoped that this would be visible after melting. The other peaks that disappear are due to short-range order of ≈15 units.

The two peaks that are visible after the melting point are at 844 and 811 cm$^{-1}$. They are the most intense regularity bands in the Raman spectrum at 160 °C. The band at 844 cm$^{-1}$ is clearly the more intense of the two above the melting point. This is because it is due to short-range order of ≈13 units. The less intense band (in the melt) at 811 cm$^{-1}$ is due to order of ≈ 15 units long.

It must be pointed out that the band at 1461 cm$^{-1}$ is not a regularity band but was used in Figure 5.6 as it is present in most of the spectra, even at high temperatures, with the exception of the final one at 210 °C.

It is clearly visible from the plot that as the temperature approaches ≈10°C below the melting point that the disorder in the crystalline region is starting to increase. As the melting point is passed, the peak is still broadening and shifting as the unit cell is expanding and the number of defects increases rapidly. There is a massive rise in entropy at the melting point as the crystalline regions become disordered. It is also possible to see that as the temperature moves to ≈10 °C above the melting point the shift is not so marked. This implies that the unit cell has been destroyed and the polymer is disordered.The implication of these observations is that at temperatures just above the melting point, i.e. 5-10 °C there is still some order in certain regions of the melt. This therefore results in the ability to observe short range order in iPP at temperatures just above the melting point.

It is possible to conclude that at 1 °C above the melting point the polymer melt contains some regions of short-range order of at least 15 units long. As the temperature is increased to 5 °C above the melting point the short-range order drops from 15 units towards 13 units. At above 10 °C of the melting point the short-range order has dropped below 13 resulting in the disappearance of the band at 844 $cm^{-1}$.

### 5.3.2 Results for polyethylene terephthalate

The FT-Raman spectra of PET at varying temperatures are shown in Figure 5.7.

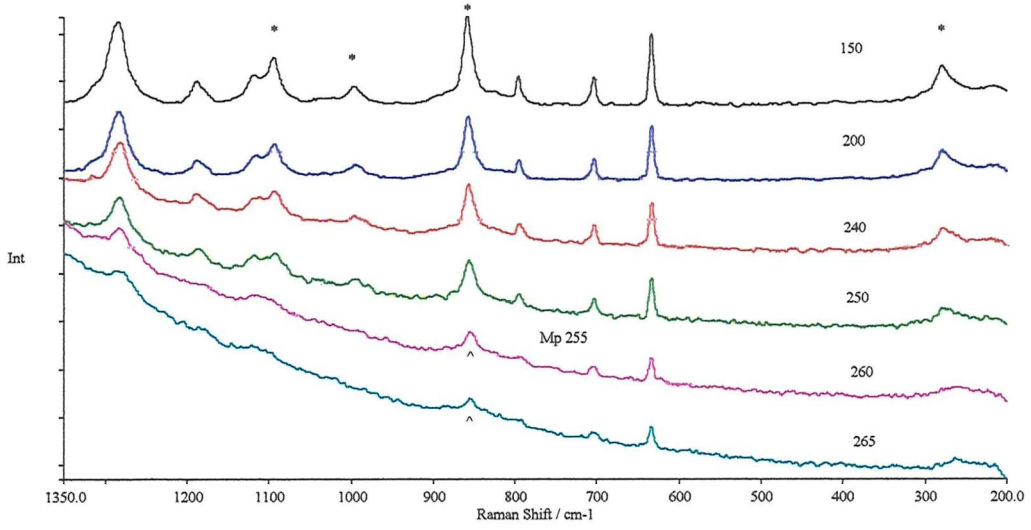


**Figure 5.7:** *The Raman spectra of PET at various temperatures. Bands due to long range order are labelled *, those visible above the melting point are labelled ^. All temperatures are in °C. The background rise above 240 °C is due to black body emission.*

As in polypropylene, peak broadening and peak shifting are clearly visible. This is probably again due to the expansion of the unit cell and an increase in the number of defects in the crystalline region. For PET this is accompanied by a *trans* to *gauche* transition. The more disorder the lower the degree of crystallinity and hence the higher the number of *gauche* conformers.

The peak shift for the band at ≈ 1615 $cm^{-1}$ is clearly seen in Figure 5.8.

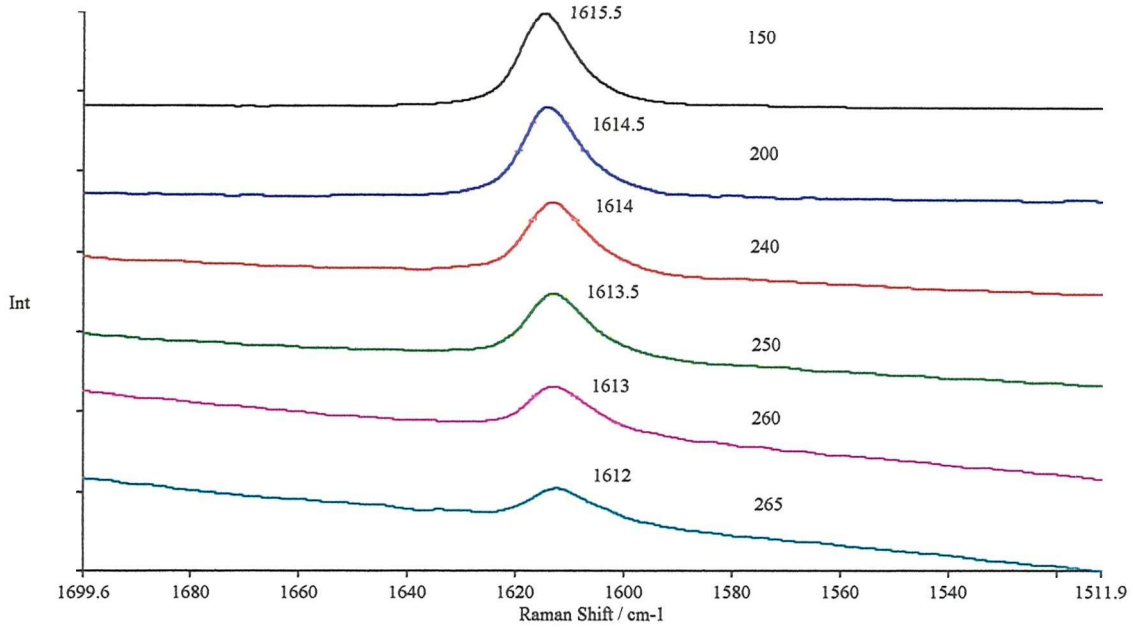


**Figure 5.8:** *The FT-Raman spectrum of the PET band at ~1615 $cm^{-1}$. A shift is clearly visible.*

A plot of wavenumber versus the increase in temperature can be seen in Figure 5.9. There are four Raman bands indicative of long range order in PET, 1096, 1000, 857 and 278 $cm^{-1}$. It was hoped that these would provide an indication of short-range order in the melt.

As with iPP the weaker bands which could have indicated short range order in the melt broadened and disappeared. The most intense of these bands, at 857 $cm^{-1}$, is clearly visible up to and slightly above the melting point. This indicates the presence of some short-range order in the melt of PET. The band is clearly visible at the melting point and 5 °C above it.

The tailing visible on the 1615 $cm^{-1}$ band as the temperature is increased is probably due to the breaking of the hydrogen bonds between the oxygen and hydrogen which are held in close proximity in the crystalline phase but are able to move more freely in the disordered phase.

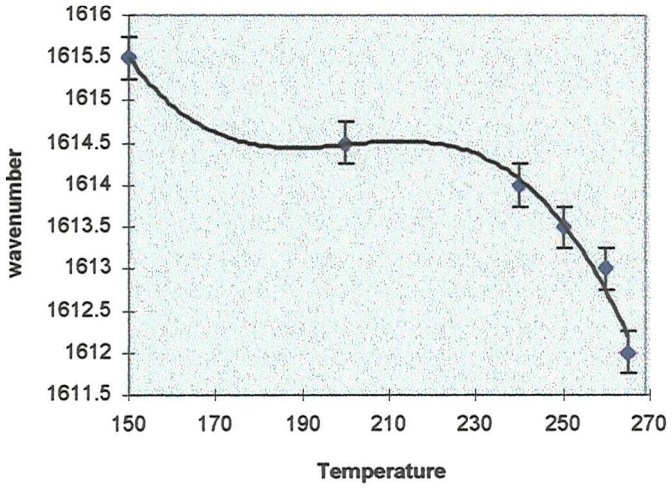


**Figure 5.9:** *Plot of wavenumber ($cm^{-1}$) versus temperature(°C) for the PET Raman band at ~1615 $cm^{-1}$. The melting point is at 255 °C.*

## 5.3.3 Comparison of results for iPP and PET

There are clear similarities between Figure 9 and Figure 6. As the melting point is approached the peak begins to shift rapidly due to both an expansion of the unit cell and a dramatic increase in the number of defects. This continues through and beyond the melting point. It is noteworthy that decrease in frequency (from 172 °C in polypropylene and 230 °C in PET) coincides with the limit of the annealing range.

As with iPP it is possible that there could be some order present just above the melting point which may be visible using FT-Raman spectroscopy. Unfortunately, it proved impossible to obtain spectra at temperatures above 265 °C due to black body radiation.

In an ideal study it would have been possible to raise the temperature until the peak was no longer visible but this was not feasible. It was also impossible to ascertain the number of PET units that are required to make up the short-range order. The supporting research has not been published for the peak in question in this case.

If short range order (i.e. concentrated areas of trans isomers in a predominantly gauche environment), is visible in the melt then it is reasonable to assume that higher than expected trans content in local domains (but not integrated over the whole) may be present in the amorphous regions of the solid polymer. This suggests that a mesomorphic region as described in references [30,31] is present in solid PET.

## 5.4 Conclusions

The first FT-Raman spectra of these two commercially important polymers at temperatures above 200 °C are reported. Evidence was obtained that indicates the presence of regularity bands in iPP at temperatures up to 5 °C above the melting point of the polymer. Studies on PET revealed some short-range order above its melting point. This adds to the argument for the presence of a mesomorphic phase in the solid.

Further work must include an attempt to increase the maximum temperature at which FT-Raman spectra can be obtained by using long wave blocking edge filters which transmit most of the shorter-wave Raman scattering or by using dynamic methods such as those demonstrated by Bennett as discussed earlier. Further study should be devoted to a closer examination of the region surrounding the melting point of polymers in order to establish the amount of order present and at what temperatures.

The observation of regularity bands above the melting point is highly significant. In all laser focused Raman experiments, whether they use visible or NIR excitation, the point of illumination is always heated to some extent. In this case heating is predicted to amount to a degree or two. If this is so order discussed is even more marked than it appears, as the local temperature at the point of analysis will be higher than that of the cell itself.

## References


1. Z. Mencik, *J.Macromol.Sci.Phys.*, **B6**, 101, (1972).
2. G.V. Fraser, P.J. Hendra, D.S. Watson, M.J. Gall, H.A. Willis, M.E.A. Cudby, *Spectrochim. Acta Part A*, **29A**, 1525, (1973).
3. H. Tadokoro, M. Kobayashi, M. Ukita, K. Yasufuku, S. Murahashi, T. Toru, *J.Chem.Phy.*, **42**, 1432, (1965).
4. G. Zerbi, L. Piseri, *J.Chem.Phys.*, **49**, 3840, (1968).
5. R.G. Synder, J.H. Schachtschneider, *Spectrocim. Acta Part A*, **20**, 853, (1964).
6. M.C. Tobin, *J.Phys.Chem.*, **64**, 216, (1960).
7. T.I. Malakov, V.N. Nikitin, *Opt. Specktrosk.*, **17**, 452, (1964).
8. R.F. Schaufele, *J. Opt. Soc. Amer.*, **57**, 105, (1967).
9. P.D. Vasco, J.L. Koenig, *Macromolecules*, **3**, 597, (1970).
10. M. Arruebarrena de Baez, P.J. Hendra, M. Judkins, *Spectrochim. Acta Part A*, **51A**, 2117, (1995).
11. G. Natta, P.Corradini, M. Cesari, *Atti. Accad. Nazl. Lincei Rend. Classe Sci, Fis. Mat. Nat.*, **21**, 365, (1956).
12. S. Krimm, *Fortschr. Hochpolymer Forscgh.*, **2**, 135, (1960).
13. G. Zerbi, F. Ciampelli, V.J. Zamboni, *J. Polym. Sci.*, **7**, 141, (1963).
14. T. Miyazawa, Y. Ideguchi, *Bull. Chem. Soc. Jpn.*, **37**, 1065, (1964).
15. T. Miyazawa, K. Fukushima, Y. Ideguchi, *Bull. Chem. Soc. Jpn.*, **B1 385**, (1963).
16. G.W. Chantry, J.W. Flemming, G.W.F. Pardoe, W. Reddish, H.A. Willis, *Infra-red Phys.*, **11**, 109, (1971).
17. D.R. Beckett, J.M. Chalmers, M.W. Mackenzie, H.A. Willis, H.G.M. Edwards, J.S. Lees, D.A. Long, *Eur. Polym. J.*, **21**, 849, (1985).
18. G.J. Stafford, H.R. Danner, H. Boutin, M. Berger, *J. Chem. Phys.*, **40**, 1426, (1964).
19. T. Yasukawa, M. Kimura, N. Watanabe, M. Yamada, *J. Chem. Phys.*, **55**, 983, (1971).
20. Y.V. Kishin, L.A. Rishina, *Eur. Polym. J.*, **12**, 757, (1976).
21. M. Kobayashi, K. Akita, H. Tadokoro, *Makromol. Chem.*, **118**, 324, (1968).
22. T. Miyamoto, H. Inagaki, *J. Polym. Sci., A2*, **7**, 963, (1969).
23. L.A. Hanna, P.J. Hendra, W. Maddams, H.A. Willis, V. Zichy, M.E.A. Cudby, *Polymer*, **29**, 1843, (1988).

24. G. Zerbi, M. Gussoni, F. Ciampelli, *Spectrochim. Acta, Part A*, **23A**, 301, (1967).
25. P.J. Hendra, D.B. Morris, R.D. Sang, H.A. Willis, *Polymer*, **23**, 9, (1982).
26. P.G. Schmidt, *J. Polym. Sci.*, **A1**, 1271, (1963).
27. W.H. Cobbs, R.L. Burton, *J. Polym. Sci.*, **70**, 275, (1953).
28. A. Miyake, *J. Polym. Sci.*, **38**, 497, (1959).
29. G.E. McGraw, in: C.D. Craver (Ed.), *Polymer Characterisation, Interdisciplinary Approaches*, Plenum Press, New York, (1971).
30. Y. Y. Fu, W.R. Busing, Y. Jin, K.A. Affholter, B. Wunderlich, *Macromol. Chem. Phys.*, **195**, 803, (1994).
31. A. Ruvolo-Filho, G.M. de Carvalho, J. Macromol. Sci. Phys., B35, 2, 255, (1996).
32. P. Gillet, *Phys. Chem. Minerals*, **23**, 263, (1996).
33. N. Umesaki, M. Takahashi, M. Tatsumisago, T. Minami, *J. Non Crys. Solids*, **225**, 205, (1996).
34. Y. K. Voronko, A.B. Kudryavstev, V.V. Osiko, A.A. Sobol, *Growth of Crystals*, **16**, 199, (1988).
35. S.J.A. Pope, Y.D. West, *Spectrochim. Acta, Part A*, **51A**, 2027, (1995).
36. C.J. Petty, R. Bennett, *Spectrochim. Acta, Part A*, **41A**, 331, (1990).
37. D.J. Cutler, C.J. Petty, *Spectrochim Acta, Part A*, **47A**, 1157, (1991).

# Chapter 6

# Conclusion

# Chapter 6

# Conclusion

The Southampton group has been concerned for very many years with developing applications of infrared spectroscopy and Raman spectroscopy in chemical analysis. Over the last decade, interest has focussed on FT-infrared and FT-Raman applications. As has been normal practice in the group, I was asked to contribute to this ongoing effort in two specific areas – one chemical and analytical, the other instrumental.

Polysulfide sealants are used extensively in the aerospace industry for the sealing of integral fuel tanks. Degradation of the sealant over the lifetime of an aircraft leads to the eventually leakage of fuel and results in very expensive repairs and a loss of earnings while the aircraft is on the ground. Therefore aircraft manufacturers are greatly concerned with the problem and are seeking solutions.

I was asked to examine the degradation of a typical polysulfide sealant and the factors that lead to this degradation. The different factors that the sealant is exposed to during its lifetime were established. Subjecting samples of the sealant to accelerated testing demonstrated that aircraft fuel actually leached material from the sealant. I suggest that, in fact, polymer oligomers are extracted and that over time leak pathways through the sealant result as more and more material is leached out. The sealant swells when exposed to aircraft fuel so that when a sealant is dried out (during repairs) more leaks appear afterwards before the sealant is once again swollen by fuel.

I also demonstrated that the pretreatment method of solvent wiping to clean surfaces before the application of the sealant is worthless. That this would be detrimental to sealant adhesion must be investigated.

Other follow up work should include an investigation to determine the effects that water and water/fuel mixture would have during accelerated testing of the sealant.

Research should also focus on producing a sealant which does not leach material on exposure to aircraft fuel.

Hot samples emit radiation. The emitted radiation does not appear in the visible until 600 °C is reached, but in the near infrared it is evident at temperatures much lower than this. By 180 °C the emission becomes a real nuisance in the region of the near infrared explored in FT-Raman spectroscopy. I was asked to explore the use of filters as a method of extending the temperature range above 200 °C. Specifically the samples of interest were the polymers polypropylene and poly(ethylene terephthalate) where the structure below, at and immediately above their melting points.

I was able to demonstrate that, using filters, FT-Raman spectra could be recorded at temperatures up to 265 °C. Above this, the background becomes unacceptable intense. It is possible to record Raman spectra of isotactic polypropylene up to and through the melting point. It was concluded that regularity bands are present up to 5 °C above the melting point. It was also possible to record Raman spectra of poly(ethylene terephthalate). In this case there is a *trans* to *gauche* transition. Again some short range order is observed above the melting point.

Further work should include an attempt to increase the maximum temperature at which FT-Raman spectra can be obtained perhaps by using long wave blocking edge filters which transmit most of the shorter-wave Raman scattering or by using dynamic methods. Study should also include a closer examination of the region surrounding the melting point of polymers in order to establish the amount of order present and at what temperatures.